Article:
Brodie, Claire N., Sotorrios, Lia, Boyd, Timothy M. et al. (2022) Dehydropolymerization of H3B·NMeH2Mediated by Cationic Iridium(III) Precatalysts Bearing κ3-iPr-PNRP Pincer Ligands (R = H, Me): An Unexpected Inner-Sphere Mechanism. ACS Catalysis. 13050–13064. ISSN: 2155-5435

https://doi.org/10.1021/acscatal.2c03778

ACS Catalysis

pubs.acs.org/acscatalysis

Research Article

Dehydropolymerization of $H_3B{\cdot}NMeH_2$ Mediated by Cationic Iridium(III) Precatalysts Bearing κ^3-^{i}Pr-PN^{R}P Pincer Ligands (R = H, Me): An Unexpected Inner-Sphere Mechanism

Claire N. Brodie,* Lia Sotorrios, Timothy M. Boyd, Stuart A. Macgregor,* and Andrew S. Weller*

Cite This: *ACS Catal.* 2022, 12, 13050−13064

Read Online

ACCESS | Metrics & More | Article Recommendations | Supporting Information

ABSTRACT: The dehydropolymerization of $H_3B{\cdot}NMeH_2$ to form *N*-methylpolyaminoborane using neutral and cationic catalysts based on the {Ir(^{i}Pr-PN^{H}P)} fragment [^{i}Pr-PN^{H}P = κ^3-($CH_2CH_2P^iPr_2$)$_2$NH] is reported. Neutral Ir(^{i}Pr-PN^{H}P)H_3 or Ir(^{i}Pr-PN^{H}P)H_2Cl precatalysts show no, or poor and unselective, activity respectively at 298 K in 1,2-$F_2C_6H_4$ solution. In contrast, addition of [$NMeH_3$][BAr$^F_4$] (Ar^F = 3,5-(CF_3)$_2C_6H_3$) to Ir(^{i}Pr-PN^{H}P)H_3 immediately starts catalysis, suggesting that a cationic catalytic manifold operates. Consistent with this, independently synthesized cationic precatalysts are active (tested between 0.5 and 2.0 mol % loading) producing poly(*N*-methylaminoborane) with M_n ∼ 40,000 g/mol, $Đ$ ∼1.5, i.e., dihydrogen/dihydride, [Ir(^{i}Pr-PN^{H}P)(H)$_2$(H_2)][BAr$^F_4$]; σ-amine-borane [Ir(^{i}Pr-PN^{H}P)(H)$_2$($H_3B{\cdot}NMe_3$)][BAr$^F_4$]; and [Ir(^{i}Pr-PN^{H}P)(H)$_2$($NMeH_2$)][BAr$^F_4$]. Density functional theory (DFT) calculations probe hydride exchange processes in two of these complexes and also show that the barrier to amine-borane dehydrogenation is lower (22.5 kcal/mol) for the cationic system compared with the neutral system (24.3 kcal/mol). The calculations show that the dehydrogenation proceeds via an inner-sphere process without metal−ligand cooperativity, and this is supported experimentally by N−Me substituted [Ir(^{i}Pr-PN^{Me}P)(H)$_2$($H_3B{\cdot}NMe_3$)][BAr$^F_4$] being an active catalyst. Key to the lower barrier calculated for the cationic system is the outer-sphere coordination of an additional $H_3B{\cdot}NMeH_2$ with the N−H group of the ligand. Experimentally, kinetic studies indicate a complex reaction manifold that shows pronounced deceleratory temporal profiles. As supported by speciation and DFT studies, a key observation is that deprotonation of [Ir(^{i}Pr-PN^{H}P)(H)$_2$(H_2)][BAr$^F_4$], formed upon amine-borane dehydrogenation, by the slow in situ formation of $NMeH_2$ (via B−N bond cleavage), results in the formation of essentially inactive Ir(^{i}Pr-PN^{H}P)H_3, with a coproduct of [$NMeH_3$]$^+$/[$H_2B(NMeH_2)_2$]$^+$. While reprotonation of Ir(^{i}Pr-PN^{H}P)H_3 results in a return to the cationic cycle, it is proposed, supported by doping experiments, that reprotonation is attenuated by entrainment of the [$NMeH_3$]$^+$/[$H_2B(NMeH_2)_2$]$^+$/catalyst in insoluble polyaminoborane. The role of [$NMeH_3$]$^+$/[$H_2B(NMeH_2)$]$^+$ as chain control agents is also noted.

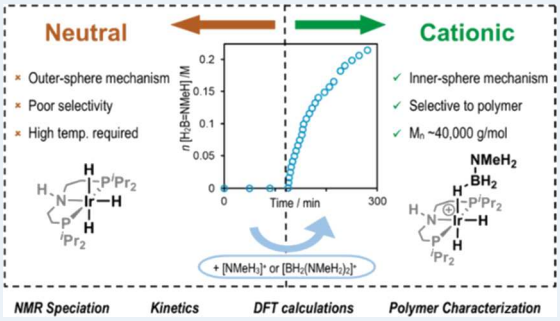

KEYWORDS: *dehydropolymerization, iridium, mechanism, amine-borane, catalyst, metal−ligand cooperativity, polymer, kinetics*

1. INTRODUCTION

The dehydropolymerization of primary amine-boranes,[1−5] $H_3B{\cdot}NRH_2$ (R = alkyl), allows for the atom-efficient formation of main-group polymers with B−N main chain units, polyaminoboranes, $(H_2BNRH)_n$,[6−8] with H_2 as the only byproduct. Dehydropolymerization is proposed to occur through a two-step process, in a cascade-like[9] polymerization, Scheme 1. Dehydrogenation of the amine-borane premonomer first forms a transient[10,11] aminoborane monomer that then undergoes polymer chain propagation.[10,12−14] Since the initial report[1] by Manners in 2008 that Ir(POCOP)H_2 [POCOP = κ^3-(OP^tBu_2)$_2C_6H_3$] can act as an efficient amine-borane dehydropolymerization catalyst to give high-molecular-weight polyaminoborane, the use of various transition metal catalysts based upon Ir,[15] Ru,[16] Fe,[17−19] Co,[20−23] Rh,[24−29] Zr,[30] and Ti[31,32] has been demonstrated. Polyaminoboranes are isosteric with simple polyolefins, and in addition to the fundamental

Scheme 1. Amine-Borane Dehydropolymerization

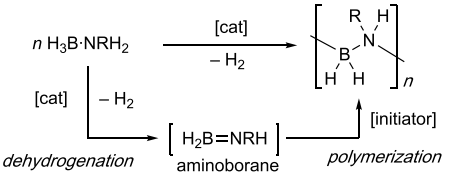

Received: August 1, 2022
Revised: September 27, 2022

interest that surrounds such main-group polymeric materials,[8,33] they have potential piezoelectric applications[34] or as polymeric precursors to BN-containing materials.[35−39]

While the precise details of chain growth processes remain to be resolved, due to the transient and highly reactive nature of aminoborane monomers, the mechanism is likely a rapid head-to-tail chain growth polymerization initiated by the catalyst or other Lewis-bases: as first proposed by Manners[5] and Baker,[40] and supported by computational studies,[12,41] polymer growth kinetics,[5,27] and analogous phosphinoborane polymerizations.[14] In contrast, the understanding of the initial catalytic dehydrogenation of amine-boranes to give aminoboranes is better developed, as reaction progress can be conveniently followed by H_2 evolution as a proxy for aminoborane generation, catalyst speciation, and isotope labeling studies. There are three accepted pathways for dehydrogenation, Scheme 2: (A) stepwise or concerted

Scheme 2. Pathways for Amine-Borane Dehydrogenation: (A) Inner Sphere, (B) MLC, and (C) Hydride Transfer

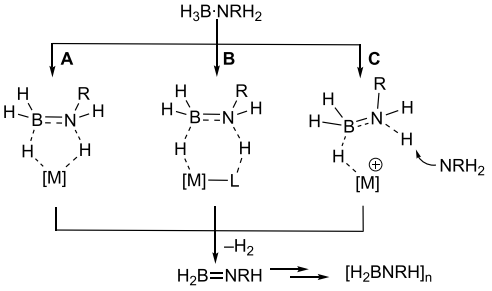

inner-sphere BH/NH activation;[42−45] (B) metal−ligand cooperative (MLC) processes;[16,19,46,47] and (C) amine-promoted hydride transfer at a cationic metal center, followed by reprotonation to release H_2.[48−50]

Group 8 catalysts with the ^{i}Pr-PN^{H}P ligand [^{i}Pr-PN^{H}P = {κ^3-($CH_2CH_2P^iPr_2$)$_2$NH] have been reported by Schneider and Beweries to be particularity effective for the dehydrogenation of amine-boranes, operating via MLC mechanisms (i.e., B, Scheme 2). Examples include Ru(^{i}Pr-PN^{H}P)(H)$_2$PMe$_3$,[16,51] Fe(^{i}Pr-PNP)H(CO),[18,19] and Fe(^{i}Pr-PN^{H}P)(H)(HBH_3)(CO).[17] We also have recently reported the use of this ligand with group 9 systems for the dehydropolymerization of $H_3B{\cdot}NMeH_2$ to form *N*-methyl polyaminoborane. While the precatalyst Co(^{i}Pr-PN^{H}P)Cl_2[20] promotes rapid and selective dehydropolymerization, mechanistic studies were frustrated because of the paramagnetic nature of the species present, although the NMe variant, Co(^{i}Pr-PN^{Me}P)Cl_2, was inactive suggesting a cooperative ligand mechanism. In contrast, by using diamagnetic [Rh(^{i}Pr-PN^{H}P)(NBD)]Cl as a cationic precatalyst, the generation of an active neutral dehydrogenation catalyst, Rh(^{i}Pr-PN^{H}P)H_3, was revealed,[52] and dehydrogenation operates via a cooperative ligand mechanism. It was proposed that Rh(^{i}Pr-PN^{H}P)H_3 forms from an $NMeH_2$-promoted hydride transfer (C, Scheme 2)[48,49] from $H_3B{\cdot}NMeH_2$ to in situ generated Rh(^{i}Pr-PN^{H}P)H_2Cl. The eventual boronium coproduct of this, [$H_2B(NMeH_2)_2$]Cl, was also shown to act as a chain-transfer agent that modifies the degree of polymerization in the resulting polyaminoboranes. This system can also be used at low catalyst loadings (0.01 mol %) to selectively produce $(H_2BNMeH)_n$ in a controlled polymerization, on a scale (10 g) that allows for the study of the resulting materials and processing properties.

Given that Rh(^{i}Pr-PN^{H}P)H_3 is an active catalyst and that the iridium congener Ir(^{i}Pr-PN^{H}P)H_3, reported by Abdur-Rashid,[53] promotes a variety of outer-sphere hydrogen transfer processes,[54−56] were we interested to explore whether neutral Ir(^{i}Pr-PN^{H}P) complexes also promote rapid and selective amine-borane dehydropolymerization. Here, we report that, surprisingly, under the conditions used they are poor to inactive catalysts for the dehydropolymerization of $H_3B{\cdot}NMeH_2$. Instead cationic species, such as the σ-amine-borane complex [Ir(^{i}Pr-PN^{H}P)H_2($H_3B{\cdot}NMe_3$)][$BAr^F{}_4$], are competent catalysts at room temperature, selectively producing $(H_2BNMeH)_n$, Scheme 3. While the resulting kinetics are

Scheme 3. This Work

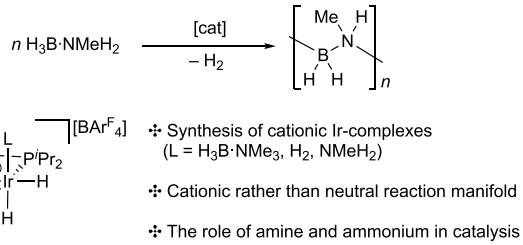

complex and suggested to be modified by polymer precipitation/coproduct or catalyst entrainment, an inner-sphere mechanism is proposed for dehydrogenation that proceeds via an asynchronous, concerted N−H/B−H activation rather than a cooperative pathway involving the ^{i}Pr-PN^{H}P ligand, in which $NMeH_2$ and ammonium, $[NMeH_3]^+$ (or its operational equivalent boronium [$H_2B(NMeH_2)_2]^+$), play a role in shuttling between observed resting states. These studies are supported and informed by independent synthesis and speciation experiments, as well as density functional theory (DFT) calculations. The NMe variant, [Ir(^{i}Pr-PN^{Me}P)H_2($H_3B{\cdot}NMe_3$)][$BAr^F{}_4$], is also a competent dehydrogenation catalyst, supporting an inner-sphere rather than an MLC mechanism. While it is well established that inner-sphere mechanisms can still operate with ligands that can support MLC processes,[57−59] for amine-borane dehydrogenation/dehydropolymerization this is an unexpected observation.[3,4,16−19,46,51,52,60−62] These studies again demonstrate that the mechanism of amine-borane dehydropolymerization is highly catalyst-dependent.[2]

2. RESULTS AND DISCUSSION

2.1. Trialing a Neutral Ir(^{i}Pr-PN^{H}P) Precatalyst. In our previous study,[52] we reported that the neutral complex *cis*-Rh(^{i}Pr-PN^{H}P)H_2Cl was an excellent precatalyst for $H_3B{\cdot}NMeH_2$ dehydropolymerization at room temperature, forming the active catalyst Rh(^{i}Pr-PN^{H}P)H_3 in situ. We thus first looked to the analogous iridium system *cis*-Ir(^{i}Pr-PN^{H}P)H_2Cl[53,63] (**1-H$_2$Cl**) as a precatalyst for dehydropolymerization, in THF solvent at room temperature. However, this neutral iridium complex was a poor precatalyst at 1 mol % loading, returning unreacted $H_3B{\cdot}NMeH_2$ (61%) alongside a mixture containing short-chain oligomers and the cyclic triborazane $(NMeHBH_2)_3$ after 6 h (Scheme 4). In contrast, *cis*-Rh(^{i}Pr-PN^{H}P)H_2Cl promotes 100% conversion in ∼200 s with excellent selectivity and pseudo-zero-order kinetics for H_2 evolution.[52]

https://doi.org/10.1021/acscatal.2c03778
ACS Catal. 2022, 12, 13050−13064

Scheme 4. Difference in Reactivity between Neutral Rh (A) and Ir (B) Systems in $H_3B{\cdot}NMeH_2$ Dehydropolymerization

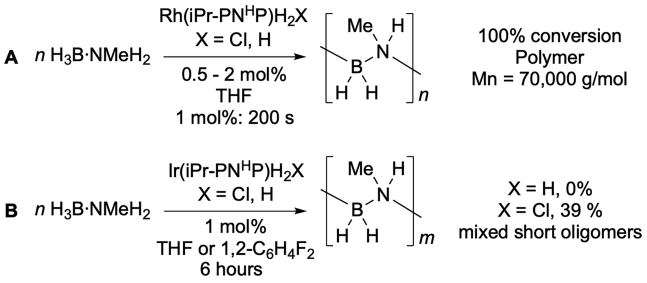

To discount whether this unexpectedly unselective and low activity of **1-H_2Cl** resulted from the inability to form the putative active species Ir(^{i}Pr-PN^{H}P)H_3, **1-H_3**, this complex was prepared independently[53] and deployed in catalysis. At 298 K, **1-H_3** showed no activity at 1 mol %, being returned unchanged after 2 h. This poor, to no, activity at room temperature for both systems shows that a neutral Ir(^{i}Pr-PN^{H}P)H_3 catalytic system is not operational for iridium. We discount an inhibitory solvent effect, as changing from THF to 1,2-$F_2C_6H_4$ solvent did not change the outcome of the reaction. No borohydride[19] or amido-borane deactivation products are observed.[17,64] Heating $H_3B{\cdot}NMeH_2$/**1-H_3** (1 mol %) to 60 °C (30 min) in 1,2-$F_2C_6H_4$ solvent did result in conversion, but this produced an ill-defined bimodal polymer/oligomer mixture as measured by gel permeation chromatography (GPC) and ^{11}B NMR spectroscopy. This result is also consistent with an early report by Fagnou and co-workers on the poor performance of *trans*-Ir(^{i}Pr-PN^{H}P)H_2Cl/K^{t}OBu for $H_3B{\cdot}NMeH_2$ dehydrogenation at 50 °C.[62] Under the same conditions but without catalyst present, $H_3B{\cdot}NMeH_2$ is unchanged.

2.2. Catalysis by Cationic Species. Given this poor and unselective reactivity of the neutral systems, we turned our attention to the investigation of cationic iridium catalysts for $H_3B{\cdot}NMeH_2$ dehydropolymerization to see if this opened up a productive mechanistic pathway. While **1-H_3** is inactive at room temperature (1 mol %, 1,2-$F_2C_6H_4$, 0.223 M $H_3B{\cdot}NMeH_2$), addition of two equivalents of [$NMeH_3$][BAr^F_4] after 110 min of inactivity immediately starts productive turnover, as measured by H_2 evolution (eudiometrically), Figure 1A. Catalysis proceeds to completion with one equivalent of H_2 released, at an initial rate of 2.3(3) × 10^{-4} M/s. Polyaminoborane $(H_2BNMeH)_n$ is produced selectively

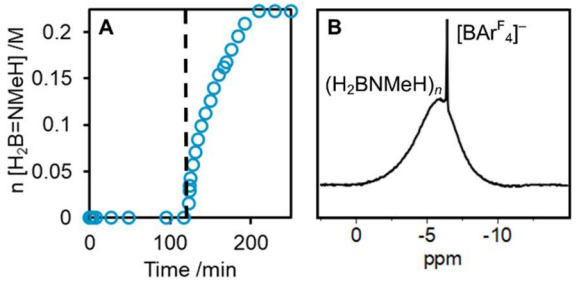

Figure 1. (A) Dehydropolymerization of $H_3B{\cdot}NMeH_2$ (0.223 M in 1,2-$F_2C_6H_4$) at 1 mol % **1-H_3**. $H_2B{=}NMeH$ equivalents formed from H_2 evolution (eudiometer). Dashed line indicated addition of 2 equiv. [$NMeH_3$][BAr^F_4]. (B) Baseline-corrected ^{11}B NMR spectrum of the reaction mixture postcatalysis.

(92%) and can be isolated in moderate yield (44%) as a white solid by precipitation into hexanes. ^{11}B NMR spectroscopy of the postcatalysis mixture shows the characteristic broad signal at δ −5.90, Figure 1B,[5] alongside a sharper signal for [BAr^F_4]$^-$ at slightly higher field. GPC analysis (THF, 0.1 w/w% [NBu_4]Br, relative to polystyrene standards) shows a monomodal distribution M_n = 18,700 g/mol ($Đ$ = 1.3). Very similar results are obtained when boronium [$H_2B(NMeH_2)_2$]-[BAr^F_4] is used instead, reflecting that that these two proton sources are interchangeable in this system. A control experiment shows that addition of [$NMeH_3$][BAr^F_4] to $H_3B{\cdot}NMeH_2$ did not result in reaction.[65]

As discussed later (Section 2.9), addition of [$NMeH_3$]-[BAr^F_4] to **1-H_3** results in the clean formation of the cationic amine adduct [Ir(^{i}Pr-PN^{H}P)($NMeH_2$)$(H)_2$][BAr^F_4], [**1-$NMeH_2$**][**BAr^F_4**]. This supports ammonium (or boronium) in promoting the movement from an inactive neutral system to an active cationic manifold. As it is likely that cationic amine-borane σ-complexes are intermediates in catalysis, as demonstrated previously,[3,4,43,66] the synthesis of suitable precursors is described next.

2.3. Synthesis of [Ir(^{i}Pr-PN^{H}P)(COD)][BAr^F_4]. An entry point to cationic σ-amine-borane complexes is labile dihydrogen complexes.[67,68] A suitable precursor to such a complex is the conveniently synthesized [Ir(^{i}Pr-PN^{H}P)(η^2,η^2-COD)][BAr^F_4] [**1-COD**][**BAr^F_4**] (Scheme 5). [**1-COD**]-

Scheme 5. Synthesis of [1-COD][BAr^F_4]

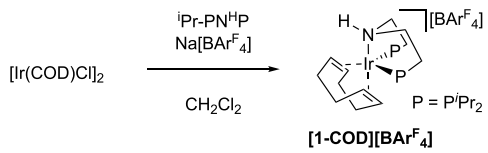

[**BAr^F_4**] was isolated as an analytically pure crystalline material in 87% yield and characterized by NMR spectroscopy and single-crystal X-ray diffraction (see Supporting Materials). These data show a κ^3-P,N,P-coordination of the tridentate ligand and η^2,η^2-coordination of the diene, at a *pseudo*-trigonal bipyramidal Ir center with C_s symmetry. In the ^{1}H NMR spectrum, four distinct isopropyl methyl environments and two alkene signals are observed, with a single environment observed in the ^{31}P{^{1}H} NMR spectrum.

2.4. Synthesis of [Ir(^{i}Pr-PN^{H}P)$(H)_2(H_2)$][BAr^F_4]. Addition of hydrogen (2 bar) to a CD_2Cl_2 solution of [**1-COD**][**BAr^F_4**] in a J. Youngs NMR tube results in the slow (36 h) but quantitative hydrogenation of the coordinated COD to give free cyclooctane (δ_H 1.53). The accompanying organometallic species formed was characterized in situ as [Ir(^{i}Pr-PN^{H}P)-$(H)_2(H_2)$][BAr^F_4] [**1-H_4**][**BAr^F_4**], Scheme 6A. In the room-temperature ^{1}H NMR spectrum (500 MHz, CD_2Cl_2), a broad triplet at δ −10.17 [J(PH) = 7.6 Hz] of relative integral 4H is observed, assigned to hydride ligands, which sharpens to a singlet upon ^{31}P decoupling. T_1 is measured as 232(8) ms at this temperature for the hydride signal. This single hydride environment indicates that rapid hydride site exchange is operating at 298 K, being similar to that reported for [Ir{κ^3-NH($CH_2CH_2P^tBu_2$)$_2$}$(H)_2(H_2)$][PF_6].[69] Cooling broadens and splits this resonance, and at 185 K, it resolves into two very broad signals (fwhm ∼1000 Hz) at δ −6.57 and −13.85, each with relative integral 2H. T_1 is measured as 150(10) ms for both of these hydride signals. In the ^{31}P{^{1}H} NMR

https://doi.org/10.1021/acscatal.2c03778
ACS Catal. 2022, 12, 13050−13064

Scheme 6. (A) [1-H$_4$][BAr$^F_4$] Synthesis and (B) Fluxionality[a]

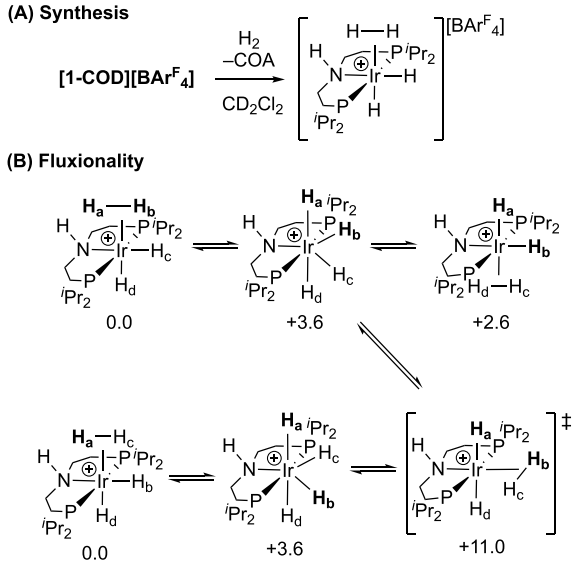

[a][BAr$^F_4$]$^-$ anions are not shown. DFT-computed free energies (kcal/mol) for stationary points along the exchange pathway are also indicated. Level of theory: BP86[D3BJ,CH$_2$Cl$_2$]/Def2TZVP//BP86/SDD (Ir, P, with polarization on P); 6-31G** on all other atoms.

spectrum, a single peak is observed at δ 53.7 which does not change significantly on cooling.

The observation of two hydride environments (albeit broad) at low temperature is consistent with a low-energy process in which the hydrogen atoms remain as distinct pairs that do not cross the IrP$_2$N plane and are undergoing site exchange within each pair via H$_2$ rotation (i.e., H$_a$/H$_b$ and H$_c$/H$_d$, Scheme 6B). DFT calculations indicate a very low barrier of 3.6 kcal/mol for this process (see Supporting Materials for full details).[70] Similar behavior has been noted for Ir(P^{i}Pr$_3$)$_2$ClH$_2$(H$_2$).[71,72] At higher temperatures, exchange between all four hydrides becomes accessible, which results in the dihydrogen ligand moving from being *syn* to *anti* with respect to the N−H group. Calculations suggest that this occurs through a *trans*-dihydride dihydrogen transition state that corresponds to rotation of the dihydrogen moiety. A higher barrier of 11.0 kcal/mol is computed for this exchange process. Consistent with a Ir(V) tetrahydride being a common intermediate is the measured T$_1$ time (150 ms), which would be expected to be much shorter (<30 ms) for an alternative bis-dihydrogen Ir(I) intermediate.[73] MXL$_2$(H)$_4$ complexes are known to be highly fluxional, with potential energy surfaces where tetrahydride and dihydrogen/dihydride structures are close in energy.[74] Removal of the hydrogen atmosphere from [**1-H$_4$**][**BAr$^F_4$**] prepared in situ results in loss of H$_2$ (~40% after 10 min) and decomposition.

2.5. Synthesis of [Ir(^{i}Pr-PN^{H}P)(H)$_2$(H$_3$B·NMe$_3$)][BAr$^F_4$] and H/D Exchange with D$_2$. While decomposition on removal of a H$_2$ atmosphere makes [**1-H$_4$**][**BAr$^F_4$**] less suitable to use as a practical and weighable precatalyst, it is an intermediate in the formation of a more tractable complex, the amine-borane adduct [Ir(^{i}Pr-PN^{H}P)(H)$_2$(H$_3$B·NMe$_3$)]-[BAr$^F_4$], [**1-H$_3$B·NMe$_3$**][**BAr$^F_4$**]. The tertiary amine-borane H$_3$B·NMe$_3$ was chosen to prevent unwanted onward dehydrocoupling from N−H activation. Addition of 1 equivalent of H$_3$B·NMe$_3$ to a solution of [**1-H$_4$**][**BAr$^F_4$**] results in the rapid (time of mixing) and quantitative conversion to [**1-H$_3$B·NMe$_3$**][**BAr$^F_4$**] and the release of H$_2$ (δ_H 4.5). On a preparative scale, addition of H$_3$B·NMe$_3$ to [**1-COD**][**BAr$^F_4$**] under a hydrogen atmosphere (2 bar, 20 h, unoptimized) allows for the quantitative formation of [**1-H$_3$B·NMe$_3$**][**BAr$^F_4$**], which was isolated in good (76%) yield as analytically pure colorless crystals. The solid-state structure, as determined by single-crystal X-ray diffraction, is presented in Figure 2. This shows a *cis*-dihydride and *mer*-κ^3-^{i}Pr-PN^{H}P

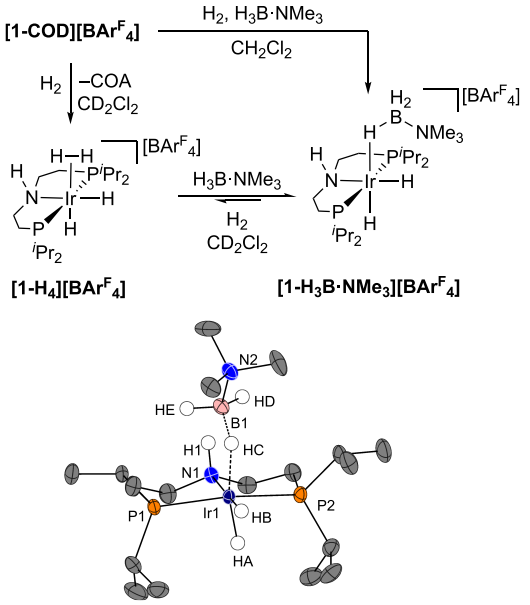

Figure 2. Preparation and molecular structure of [**1-H$_3$B·NMe$_3$**]-[**BAr$^F_4$**]. Anion not shown. Displacement ellipsoids at 50% probability level. Selected bond angles (°) and bond lengths (Å): Ir1···B1, 2.723(7); Ir1−HA, 1.45(6); Ir1−HB, 1.50(4); Ir1−HC, 1.73(6); Ir1−P1, 2.286(2); Ir1−P2, 2.280(2); Ir1−N1, 2.203(4); B1−N2, 1.61(1); P1−Ir1−P2, 165.38(6); HA−Ir1−HC, 164(3); Ir1−HC−B1, 134(4).

ligand arrangement around the metal center. Hydrogen atoms associated with the borane, amine and iridium-hydrides were located in the final difference map. These structural data show an η^1-bound H$_3$B·NMe$_3$, as indicated by a long Ir···B distance [2.723(7) Å] and open Ir−H−B angle [Ir1−HC−B1 134(4)°].[75−77] There is one B−H in a close approach to the Ir center [Ir1−HC 1.73(6) Å]. The borane is situated *syn* to the N−H group with the N−H proton bifurcating the two B−H groups [HD and HE]. A noncovalent interaction plot (see Figure S70) suggests the presence of some weak B−H···H−N interaction although the H···H distances are longer than those of conventional dihydrogen bonds (>2.29 Å).[78]

In the ^{1}H NMR spectrum at 298 K (CD$_2$Cl$_2$), the borane is observed as a broad resonance at δ −2.18, relative integral 3H. Cooling to 183 K results in this peak resolving into two signals at δ 1.87 (br) and δ −11.07 (1 H), corresponding to terminal and bridging B−H and Ir···H−B environments, respectively. At 298 K, the Ir-hydride resonances are observed at δ −20.24 and δ −22.74, as triplets of doublets, which do not change significantly in their chemical shift or coupling patterns on cooling. Overall, these data indicate that a rapid exchange[79] between the bridging and terminal B−H sites occurs at room temperature on the NMR timescale that retains the relative stereochemistry of the complex. At 298 K, the N−H group is

https://doi.org/10.1021/acscatal.2c03778
ACS Catal. 2022, 12, 13050−13064

observed at δ 3.00, only slightly upfield shifted from [**1-COD**][BAr^F_4] [δ 3.47] consistent with no significant hydrogen bonding with the borane.[80]

Addition of H_2 (2 bar, CD_2Cl_2 solution) to a sample of [**1-H_3B·NMe$_3$**][BAr^F_4] results in the displacement of the σ-amine-borane ligand by dihydrogen, generating [**1-H_4**][BAr^F_4] in situ, with these two complexes observed in an 8:2 ratio, respectively. Subsequent degassing of the sample results in the quantitative reformation of [**1-H_3B·NMe$_3$**][BAr^F_4], indicating that an equilibrium operates. When [**1-H_3B·NMe$_3$**][BAr^F_4] is exposed to D_2 (1 bar, 60 min), followed by degassing, deuterium incorporation is observed in the ^{2}H NMR spectrum at both the hydride positions and the borane. $H_{2(dissolved)}$ and $HD_{(dissolved)}$ [δ_H 4.24, 1:1:1 triplet, J(HD) = 43 Hz] are also observed in the ^{1}H NMR spectrum, alongside a reduction in the relative intensity of the hydride and borane signals (~95% when compared to ^{i}Pr). There is no evidence for H/D exchange at the amine proton, which is observed at δ_H 2.97 and retains a relative integral 1H when compared to other ligand resonances. A suggested mechanism for H/D exchange informed by DFT calculations is presented in Scheme 7.

Scheme 7. Proposed Pathway for Observed H/D Exchange in [1-H_3B·NMe$_3$][BAr^F_4][a]

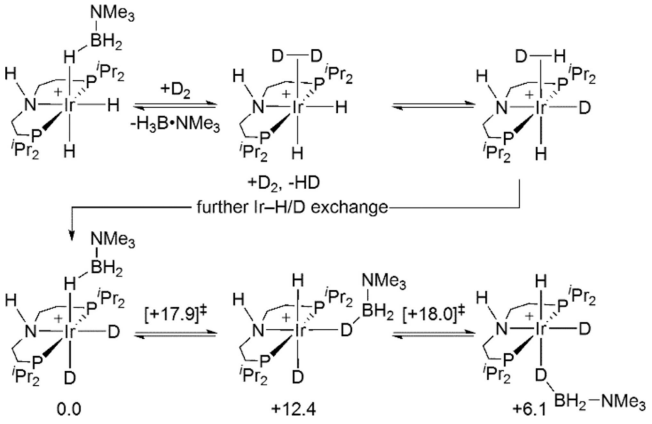

[a][BAr^F_4]$^-$ anions are not shown. DFT-computed free energies (kcal/mol) for key stationary points along the B-H(D) exchange pathway are also indicated. The full pathway involves four transition states linking three intermediates, and only the highest lying transition state energies are shown (see Figure S63 for full details). Level of theory: BP86[D3BJ,CH_2Cl_2]/Def2TZVP//BP86/SDD (Ir, P, with polarization on P); 6-31G** on all other atoms.

Displacement of $H_3B·NMe_3$ with D_2 results in [Ir(^{i}Pr-PN^{H}P)(H)$_2$D$_2$][BAr^F_4] from which H/D exchange at the Ir-hydrides occurs, as described for [**1-H_4**][BAr^F_4] (Scheme 6). Re-coordination of $H_3B·NMe_3$ followed by H/D exchange between the borane and Ir−D provides access to the B−D isotopologues. Calculations suggest that this occurs by transfer of the {BH_2·NMe_3} moiety from *syn* to *anti* to the N-H bond via a σ-$H_2DB·NMe_3$ intermediate at +12.4 kcal/mol. Facile exchange between bridging and terminal B−H(D) bonds and reversing the transfer of the {BHD·NMe_3} unit to the original position *syn* to the N-H bond complexes the exchange with an overall barrier of 18 kcal/mol. Similar H/D exchange processes have been experimentally and computationally studied for [Ir(PCy_3)$_2$(H)$_2$($H_3B·NMe_3$)][BAr^F_4].[79] While the observation of H/D exchange suggests that B−H bond activation at the Ir center may play an important role in the overall mechanism of dehydrogenation, ultimately we show this to proceed by N−*H* transfer to a hydride ligand trans to the NH ligand that then induces B−H cleavage and aminoborane loss (vide infra).[81]

2.6. Dehydropolymerization of $H_3B·NMeH_2$. Initial screening of the cationic ^{i}Pr-PN^{H}P-containing complexes [**1-COD**][BAr^F_4], [**1-H_3B·NMe$_3$**][BAr^F_4], and in situ prepared [**1-H_4**][BAr^F_4] for the dehydropolymerization of methylamine-borane, $H_3B·NMeH_2$, was carried out at 1 mol % catalyst loading in 1,2-$F_2C_6H_4$ solution (0.223 M $H_3B·NMeH_2$). Precatalyst [**1-COD**][BAr^F_4] showed no activity, in contrast to the analogous Rh system, where [Rh(κ^3-{($CH_2CH_2P^iPr_2$)$_2$NH}(NBD)]Cl was observed to be an excellent precatalyst, albeit after an induction period to form the active catalyst Rh(^{i}Pr-PN^{H}P)H_3.[52] Both [**1-H_3B·NMe$_3$**]-[BAr^F_4] and in situ prepared [**1-H_4**][BAr^F_4] are competent, but rather slow, precatalysts (Table 1), promoting quantitative

Table 1. Dehydropolymerization of $H_3B·NMeH_2$ Using Different Cationic Precursors[a]

catalyst	time/h	M_n[b]/(g/mol)	conv./%[c] (sel./%)	yield/%
[1-COD][BAr^F_4]	16		0	
[1-H_4][BAr^F_4][d]	5	35,100	99 (99)	79
[1-H_3B·NMe_3][BAr^F_4]	6	39,200	100 (97)	55
[1-H_3B·NMe_3][BAr^F_4][d]	6	45,100	99 (98)	60
[1-H_3B·NMe_3][BAr^F_4][e]	6	4800	87 (73)	23
[1-H_3B·NMe_3][BAr^F_4][f]	2	[g]	30[h]	

[a]Experimental conditions: 1 mol % cat., 0.223 M $H_3B·NMeH_2$ in 1,2-$F_2C_6H_4$ under a flow of Ar. [b]GPC analysis compared to polystyrene standards. $Đ$ for all samples measured between 1.5 and 1.7. [c]Conversion by ^{11}B NMR spectroscopy (selectivity). [d]Eudiometric conditions, jacketed-Schlenk flask at 293 K. [e]Sealed ampule. [f]In THF under eudiometric conditions. [g]Low conversion to short-chain oligomers. [h]Estimated from H_2 evolved.

conversion to poly(*N*-methylaminoborane) $(H_2BNMeH)_n$ after 6 h. The polymer was formed selectively, however, with only trace *N*-trimethylborazine or other BN products formed, as shown by a broad signal observed in the ^{11}B NMR spectrum at δ −6.1, alongside a sharp signal at δ −6.6 for [BAr^F_4]$^-$ in the crude, unprecipitated, polymer/catalyst mixture, cf. Figure 2. Analysis of the precipitated polymer by GPC (polystyrene standards, refractive index detector) showed very similar molecular weights for polymer produced by both catalysts (M_n = 35,100 g/mol and 39,200 g/mol, respectively) with relatively narrow dispersity ($Đ$ = 1.7). Interestingly, these are significantly longer than those measured for the **1-H_3**/[$NMeH_3$][BAr^F_4] catalysis (M_n = 18,700 g/mol), which supports the role of ammonium/boronium as chain control agents in dehydropolymerization.[27,52] The GPC analysis also showed an additional, sharper, signal that has previously been identified as being due to entrained [BAr^F_4]$^-$ in the polymer sample, likely as the [$NMeH_3$]$^+$ or [$H_2B(NMeH_2)_2$]$^+$ salt.[25] The [BAr^F_4]$^-$ anion coelutes with the polymers, complicating the analysis of the molecular weight distribution, meaning that degrees of polymerization should be considered as approximate only. Signals due to the residual ^{i}Pr-PN^{H}P ligand are also observed by ^{1}H NMR spectroscopy, suggesting that the catalyst is coprecipitated with the polymer.

Using [**1-H_3B·NMe$_3$**][BAr^F_4] and performing the reaction under a flow of argon to promote the removal of H_2, or under eudiometric conditions, resulted in the generation of polyaminoborane (M_n ~ 40,000 g mol^{-1}, $Đ$ ~ 1.6), with

https://doi.org/10.1021/acscatal.2c03778
ACS Catal. 2022, 12, 13050−13064

high conversion and selectivity (97%). In contrast, performing the reaction in a sealed ampule where hydrogen pressure is allowed to build up resulted in an intractable mixture of short-chain and cyclic products, for example, *N*-methylborazine, incomplete conversion (87%) and polyaminoborane with a significantly lower molecular weight (M_n ~ 5000 g/mol) and high dispersity ($Đ$ = 2.2). This, again, demonstrates the inhibitory effect that H_2 has on dehydropolymerization in some catalyst systems.[27−29] Here, we suggest the equilibrium that was established to occur between [**1-H$_4$**][**BAr$^F_4$**] and [**1-H$_3$B·NMe$_3$**][**BAr$^F_4$**] models the conditions of catalysis using $H_3B{\cdot}NMeH_2$ under conditions that allow for build-up of H_2. This will slow the dehydrogenation to form the actual monomer, $H_2B{=}NMeH$, and thus the rate of propagation. If any chain termination/transfer is proportionally less unaffected by H_2, then the resulting degree of polymerization will be lower under closed conditions.

During the course of these dehydropolymerization reactions performed in 1,2-difluorobenzene, it was noted that the solution became visibly very turbid after ca. 10 min, as a result of polymer precipitation from solution. Qualitatively $(H_2BNMeH)_n$ is more soluble in THF than 1,2-$F_2C_6H_4$;[82] as such, the reaction was also performed in THF—a solvent that has worked well for neutral catalyst systems.[52] However, the reaction was relatively sluggish and only reached ~30% conversion before activity ceased. Investigation of the mixture postcatalysis shows the formation of the inactive trihydride, **1-H$_3$**.[83] An alternative solvent toluene has been used previously in dehydropolymerization reactions, but as $H_3B{\cdot}NMeH_2$ has a limited solubility, this potentially complicates any kinetic analysis.[18] All subsequent studies were thus carried out in 1,2-$F_2C_6H_4$ solvent, where complete conversion of $H_3B{\cdot}NMeH_2$ occurs.

2.7. Kinetics of $H_3B{\cdot}NMeH_2$ Dehydrogenation. Temporal profiles for the dehydropolymerization of $H_3B{\cdot}NMeH_2$ (0.223 M) mediated by [**1-H$_3$B·NMe$_3$**][**BAr$^F_4$**] in 1,2-$F_2C_6H_4$ solvent were obtained from hydrogen evolution measurements at various catalyst loadings (0.5−2 mol %) and are shown in Figure 3. The application of simple integrated rate laws or the VTNA methodology[84] showed that catalysis did not follow a simple rate law (Supporting Materials). Moreover, visual inspection of the temporal profiles indicated a marked deceleration with time, which appears to be more pronounced at lower loadings (i.e., 0.5 mol %). Given the precipitation of the polymer from solution noted above, and the changes in speciation throughout catalysis (vide infra), kinetic analysis was performed through application of initial rates for the very early stages of catalysis where $[H_3B{\cdot}NMeH_2]$ is high and the corresponding concentration of $(H_2BNMeH)_n$ is low.

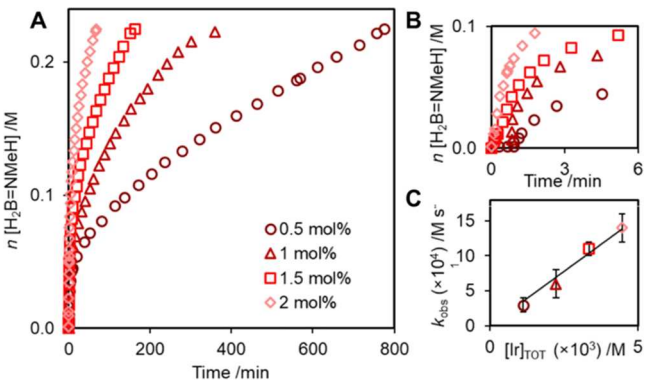

Figure 3. (A) Kinetics of dehydropolymerization of $H_3B{\cdot}NMeH_2$ using [**1-H$_3$B·NMe$_3$**][**BAr$^F_4$**] at 0.5−2 mol %. $H_2B{=}NMeH$ equivalents formed from H_2 evolution (eudiometer). Experimental conditions: 50 mg $H_3B{\cdot}NMeH_2$, 0.223 M in 1,2-$F_2C_6H_4$ (5 mL), jacketed-Schlenk flask at 293 K. (B) Early stages of catalysis. (C) First-order relationship of k_{obs} with $[Ir]_{TOT}$ at the very early stages of catalysis.

Comparison of initial rates measured as catalyst loading is varied between 0.5 and 2 mol % returns a first-order relationship in $[Ir]_{TOT}$. In each case, there is a short induction period of up to 60 s that broadly scales inversely with catalyst loading. We have previously noted similar induction periods in dehydropolymerization using cationic [Rh(Xantphos-^{i}Pr)-$(H)_2(H_3B{\cdot}NMeH_2)$][BAr$^F_4$] catalysts, and suggested trace impurities in the 1,2-$F_2C_6H_4$ solvent act to modify the catalyst systems before productive turnover starts.[25] While the initial rate measurements were qualitatively repeatable, there was also some variation between repeat runs, which may be due to trace solvent impurities or mass transfer effects due to polymer precipitation. For this reason, isotope labeling experiments were not carried out.

Polyaminoborane is produced selectively (>95%) in all cases, with close to quantitative conversion as determined by sampling of the reaction using ^{11}B NMR spectroscopy (Table 2). While the molecular weight of the resulting polymer appears to follow an inverse relationship with catalyst loading, as described for other cationic systems,[28,29] accurate measurement of the M_n is hindered by the overlapping signal from the presence of $[BAr^F_4]^-$ in the GPC trace. These data are in contrast with those obtained using the neutral Rh(^{i}Pr-PN^{H}P)H_2Cl catalyst which shows well-behaved zero-order kinetics for H_2 evolution, in THF solvent, and straightforward GPC analysis in the absence of $[BAr^F_4]^-$ that shows that M_n is invariant to catalyst loading.

2.8. In Situ Speciation Studies. Dehydropolymerization experiments were performed in a system open to the release of H_2 at 293 K, with samples taken periodically that were then analyzed using ^{1}H and ^{31}P{^{1}H} NMR spectroscopy. Measurements were carried out at 245 K (m.p. 1,2-$F_2C_6H_4$ 239 K)[85] to halt onward reactivity. A catalyst loading of 1 mol % allowed for reasonable spectra to be acquired that allowed for catalyst speciation to be investigated qualitatively. Figure 4 shows the time-course plot for H_2 evolution and ^{31}P{^{1}H} NMR spectra at various time points. At the onset of catalysis in the first 2.5 min, there are multiple species observed by ^{31}P{^{1}H} NMR spectroscopy that lie within the range of 55−48 ppm, similar to [**1-H$_3$B·NMe$_3$**][**BAr$^F_4$**] (δ 51.1). The hydride region of the ^{1}H NMR spectrum also shows multiple species (δ −20.1 to −22.4), at similar chemical shifts to those reported for $[Ir(PCy_3)_2H_2(H(BH_2NH_2)_nH][BAr^F_4]$ (n = 1 to 5) during the dehydropolymerization of $H_3B{\cdot}NH_3$.[43] A small amount of [**1-H$_4$**][**BAr$^F_4$**] is also observed (δ 53.5). A more quantitative assessment of the absolute concentrations of Ir-containing species, and thus $[Ir]_{TOT}$, was hampered by the overall low concentrations of each species, broad lower intensity peaks, and attendant low signal to noise, especially at the earlier stages of catalysis.

After 10 min, a new signal at δ 58.7 is observed which grows in as the reaction progresses and turnover slows. After 1.5 h (~60% conversion), the ^{31}P{^{1}H} NMR spectrum simplifies to show this as the major species, the appearance of which tracks the appearance of three new hydride resonances in the ^{1}H

https://doi.org/10.1021/acscatal.2c03778
ACS Catal. 2022, 12, 13050−13064

Table 2. Initial Rates for H_2 Evolution and Polymer Characterization Using $[1\text{-}H_3B{\cdot}NMe_3][BAr^F{}_4]$[a]

$[Ir]_{TOT}$/mol%	$k_{obs}/(\times 10^{-4}$ M/s)	M_n[b]/(g/mol)	$Đ$[b]	% conversion[c] (% yield)
0.5	3(1)	37,300	1.6	97(55)
1.0	6(2)	39,900	1.6	99(60)
1.5	11(1)	11,600	1.7	99(60)
2.0	14(2)	9,100	1.7	94(48)

[a]0.223 M $H_3B{\cdot}NMeH_2$ (50 mg), jacketed-Schlenk flask at 293 K, 1,2-$F_2C_6H_4$ (5 mL) using $[1\text{-}H_3B{\cdot}NMe_3][BAr^F{}_4]$. [b]Average of two runs measured by GPC relative to polystyrene standards. [c]Measured using ^{11}B NMR spectroscopy by sampling the reaction mixture (% yield of the isolated polymer).

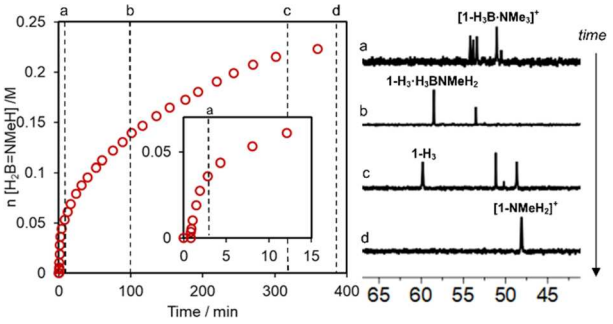

Figure 4. Temporal plot of dehydropolymerization reaction progression at 293 K (first 15 min highlighted in the inset) and corresponding $^{31}P\{^1H\}$ NMR spectra at position indicated by the dashed line recorded at 245 K: a = 2.5 min, b = 1.5 h, c = 5.1 h, d = 6.3 h. Experimental conditions: 0.223 M $H_3B{\cdot}NMeH_2$ in 1,2-$F_2C_6H_4$, 1.0 mol % $[\mathbf{1{\cdot}H_3B{\cdot}NMe_3}][\mathbf{BAr^F{}_4}]$.

NMR spectrum [δ −11.60, −12.93, and −22.67]. These are observed as broad multiplets, which collapse to broad singlets upon ^{31}P decoupling. These data are similar to those of the previously reported[53] *neutral* trihydride complex Ir(^{i}Pr-PN^{H}P)-H_3 **1-H$_3$** [δ_P = 61.5, δ_H = −11.47, −12.26, −22.25 in 1,2-$F_2C_4H_6$]. After ∼5 h (∼95% conversion), when $[H_3B{\cdot}NMeH_2]$ is very low, these signals shift slightly [δ_P = 59.8, δ_H = −11.61, −12.65, −22.63]. This change likely reports on the formation of an outer-sphere adduct at higher $[H_3B{\cdot}NMeH_2]$, that is, Ir(^{i}Pr-PN^{H}P)$H_3{\cdot}H_3B{\cdot}NMeH_2$, as shown by DFT calculations (vide infra) and is related to that observed in the analogous Rh system.[52] $[\mathbf{1\text{-}H_3B{\cdot}NMe_3}][\mathbf{BAr^F{}_4}]$ is also observed at this point, arising from coordination of the $H_3B{\cdot}NMe_3$ released at the start of catalysis. At the end of productive catalysis (ca. 6 h), there is only one Ir-containing species observed by $^{31}P\{^1H\}$ NMR spectroscopy, δ 48.0. The appearance of this signal tracks with two distinct hydride resonances at δ −20.17 and −24.14 in the corresponding ^1H NMR spectrum. This new species is identified as the cationic amine adduct [Ir(^{i}Pr-PN^{H}P)$(H)_2(NMeH_2)$][$BAr^F{}_4$], $[\mathbf{1\text{-}NMeH_2}][\mathbf{BAr^F{}_4}]$, by its independent synthesis as a crystalline solid, from addition of excess $NMeH_2$ to $[\mathbf{1\text{-}H_3B{\cdot}NMe_3}][\mathbf{BAr^F{}_4}]$ and subsequent recrystallization. $NMeH_2$ comes from B−N bond cleavage in $H_3B{\cdot}NMeH_2$, as has been commented on before.[27,48,49,52,86,87]

To summarize these in situ studies, at the early stages of catalysis a complex mixture is observed, likely [Ir(^{i}Pr-PN^{H}P)$(H)_2(L)$][$BAr^F{}_4$] adducts. As catalysis proceeds neutral **1-H$_3$** becomes dominant, to finally be replaced at the end of catalysis by the cationic amine adduct $[\mathbf{1\text{-}NMeH_2}][\mathbf{BAr^F{}_4}]$. As **1-H$_3$** does not catalyze dehydrogenation, we interpret the significant slowing in turnover as the reaction proceeds to be due to its build-up. In the next section, the relationship between these observed species is explored in more detail.

2.9. Relationship between Neutral and Cationic Species Observed during Catalysis and the Role of $NMeH_2$ and Proton Sources $[NMeH_3][BAr^F{}_4]/[H_2B(NMeH_2)_2][BAr^F{}_4]$.

As in the catalytic system $NMeH_2$ likely comes from slow B−N bond cleavage in $H_3B{\cdot}NMeH_2$, understanding the role that it plays in speciation is important. Addition of an excess (9 equiv. to $[Ir]_{TOT}$) of $H_3B{\cdot}NMe_3$ to $[\mathbf{1\text{-}NMeH_2}][\mathbf{BAr^F{}_4}]$ establishes a mixture of $[\mathbf{1\text{-}H_3B{\cdot}NMe_3}][\mathbf{BAr^F{}_4}]$:$[\mathbf{1\text{-}NMeH_2}][\mathbf{BAr^F{}_4}]$ in a ratio 0.05:0.95 showing that $NMeH_2$ binds competitively over $H_3B{\cdot}NMe_3$, but that the amine-borane adduct is still accessible. As, under the conditions used, we have shown that H_2 binds less competitively than $H_3B{\cdot}NMe_3$ (Section 2.4) this qualitatively establishes the equilibria shown in Scheme 8. Consistent with this, addition of H_2 to $[\mathbf{1\text{-}NMeH_2}][\mathbf{BAr^F{}_4}]$ does not form detectable quantities of $[\mathbf{1\text{-}H_4}][\mathbf{BAr^F{}_4}]$ by ^1H NMR spectroscopy. The equilibrium between $[\mathbf{1\text{-}H_3B{\cdot}NMe_3}][\mathbf{BAr^F{}_4}]$ and $[\mathbf{1\text{-}NMeH_2}][\mathbf{BAr^F{}_4}]$ that is biased toward amine-coordination suggests that $[\mathbf{1\text{-}NMeH_2}][\mathbf{BAr^F{}_4}]$ would be a slow catalyst. However, as $[\mathbf{1\text{-}NMeH_2}][\mathbf{BAr^F{}_4}]$ is only observed at the very end of catalysis it is unlikely that it influences the early stages of catalysis significantly. DFT-computed free energies of these three species confirm their relative stabilities (Scheme 8). Finally, addition of $[H_2B(NMeH_2)_2][BAr^F{}_4]$, or $[NMeH_3][BAr^F{}_4]$, to **1-H$_3$** forms $[\mathbf{1\text{-}NMeH_2}][\mathbf{BAr^F{}_4}]$, consistent with the initial catalytic studies reported (Section 2.2).

Scheme 8. Selected Equilibria Associated with $[\mathbf{1\text{-}H_3B{\cdot}NMe_3}]^+$[a]

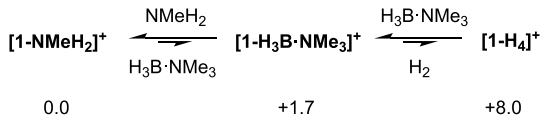

[a]$[BAr^F{}_4]^-$ anions not shown. Computed free energies (kcal/mol).

Calculations suggest that the generation of neutral **1-H$_3$** during catalysis likely occurs by initial formation of dihydrogen/dihydride $[\mathbf{1\text{-}H_4}]^+$ followed by deprotonation[88] by $NMeH_2$, Scheme 9. This entails an overall barrier of 17.9 kcal/mol and forms **1-H$_3$** and $[NMeH_3]^+$ at +12.8 kcal/mol. We propose that $[NMeH_3]^+$ is then trapped by $H_2B{=}NMeH$ (from the main catalytic cycle) to form $[H_2B(NMeH_2)_2]^+$, as this renders the formation of **1-H$_3$** more thermodynamically reasonable (ΔG = +3.5 kcal/mol).[89] Moreover, the formation of the outer-sphere adduct **1-H$_3$·H$_3$B·NMeH$_2$**, as proposed from the speciation studies and DFT calculations, makes formation even more favorable (ΔG = +1.8 kcal/mol). An alternative base-promoted hydride transfer process (cf. **C**, Scheme 2) proved inaccessible,[90] in contrast to related cationic σ-amine-borane complexes where such processes can occur with relatively low barriers.[48,49,91] The important consequence

https://doi.org/10.1021/acscatal.2c03778
ACS Catal. 2022, 12, 13050−13064

Scheme 9. Proposed Mechanism for the Formation of 1-H_3 and Its Reactivity with $[H_2B(NMeH_2)_2][BAr^F_4]$

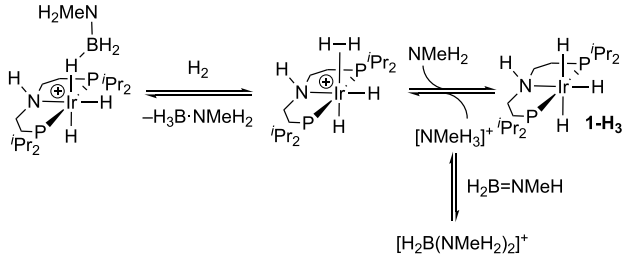

of this is that **1-H_3** must sit off-cycle, as it is not generated from coordination of $H_3B{\cdot}NMeH_2$. As $NMeH_2$ would be expected to build as catalysis proceeds, from B−N bond cleavage, **1-H_3** does not form immediately, only being observed during the slower phase of catalysis, after ∼10 min.

These stoichiometric observations are supported by catalytic experiments using different precatalysts. Initial rates were used to investigate the relative rate of turnover during the early stages of catalysis. Table 3 reports the results of these experiments. Within error, both **$[1\text{-}H_3B{\cdot}NMe_3][BAr^F_4]$** and **$[1\text{-}H_4][BAr^F_4]$** (entries 1 and 2) operate at similar initial rates, consistent with the displacement of H_2 by $H_3B{\cdot}NMeH_2$. They also produce polymers of comparable molecular weight (∼40,000 g mol^{-1}). **$[1\text{-}NMeH_2][BAr^F_4]$** promotes significantly slower turnover (∼7 times slower), entry 3, likely due to $NMeH_2$ binding competitively with amine-borane from the start of catalysis, as well as promoting the formation of **1-H_3**. Essentially, the same data are obtained if $NMeH_2$ is added to **$[1\text{-}H_3B{\cdot}NMe_3][BAr^F_4]$** (entry 4). Addition of two equivalents of $[NMeH_3][BAr^F_4]$, entry 5, results in isolated polymers of considerably lower molecular weight, consistent with the role of $[NMeH_3]^+$ as a chain control agent.

Chain control is suggested to occur by protonation of the polymeryl amine end group.[27] In support of this, added amine (entries 3 and 4) produces polymer of higher molecular weight. We have previously noted similar effects of added amine in related systems.[28] Initial rate measurements suggest that turnover may be slightly faster with added ammonium, although within error it is the same as undoped **$[1\text{-}H_3B{\cdot}NMe_3][BAr^F_4]$** and **$[1\text{-}H_4][BAr^F_4]$**. Finally, recharging the catalyst mixture with more $H_3B{\cdot}NMeH_2$ restarts catalysis, but now at a significantly slower rate (entry 6), being closer to that measured for **$[1\text{-}NMeH_2]^+$**, consistent with this complex being the final resting state.

2.10. Proposed Mechanism of Dehydrogenation. Informed by in situ NMR speciation experiments, H_2 evolution kinetics, and stoichiometric reactions, a plausible mechanism for the dehydrogenation of $H_3B{\cdot}NMeH_2$ using **$[1\text{-}H_3B{\cdot}NMe_3][BAr^F_4]$** can be suggested. The essential elements of the proposed mechanism capture the following observations:

(i) Neutral, catalytically inactive **1-H_3** sits off-cycle, and addition of $[NMeH_3][BAr^F_4]$ brings it into the productive, cationic, manifold. **1-H_3** is formed by deprotonation of **$[1\text{-}H_4][BAr^F_4]$**, rather than a base-promoted hydride transfer from a coordinated amine-borane complex.

(ii) The relative ratios of observed resting states, and thus rate of turnover, will reflect the relative proportions of $H_3B{\cdot}NMeH_2$ (decreasing with time), dissolved H_2, $NMeH_2$ (formed through B−N bond cleavage), and $[H_2B(NMeH_2)_2]^+$ or $[NMeH_3]^+$ (coproducts of the formation of **1-H_3**).

Scheme 10 shows the proposed mechanism that is also informed by DFT calculations (see below). Starting from **$[1\text{-}H_3B{\cdot}NMe_3][BAr^F_4]$** substitution with $H_3B{\cdot}NMeH_2$ generates **$[1\text{-}H_3B{\cdot}NMeH_2][BAr^F_4]$**. A concerted N-H/B−H activation then leads, via its tetrahydride isomer, to **$[1\text{-}H_4][BAr^F_4]$** with release of $H_2B{=}NMeH$ for onward polymerization, as initiated by either Ir-hydride species or free amine.[5,12,27,40,41,52] Associative $H_2/H_3B{\cdot}NMeH_2$ substitution then completes the catalytic cycle. This reaction manifold is modified by the slow formation of $NMeH_2$ from B−N bond cleavage[92] in $H_3B{\cdot}NMeH_2$. This promotes formation of off-cycle **1-H_3** via **$[1\text{-}H_4]^+$** and also produces $[H_2B(NMeH_2)_2]$-$[BAr^F_4]$ in the presence of aminoborane, $H_2B{=}NMeH$. Reprotonation by $[NMeH_3]^+$ (or $[H_2B(NMeH_2)_2]^+$) forms **$[1\text{-}NMeH_2][BAr^F_4]$**, the rate of which may be further attenuated by the formation of off-cycle adducts with $H_3B{\cdot}NMeH_2$ (as measured experimentally for $H_3B{\cdot}NMe_3/[NMe_2H_2]^+$)[49] or entrainment in precipitated polymers (vide infra). The productive catalytic cycle is returned to from **$[1\text{-}NMeH_2][BAr^F_4]$**, by coordination of $H_3B{\cdot}NMeH_2$ and replacement of $NMeH_2$. Only at the end of catalysis, when $H_3B{\cdot}NMeH_2$ is consumed, and $NMeH_2$ has built to its maximum level does the final resting state shift to the amine adduct, **$[1\text{-}NMeH_2][BAr^F_4]$**.

The key steps in this process were modeled by DFT calculations (see Figure 5A). The chemical model adopted for this study includes one outer-sphere $H_3B{\cdot}NMeH_2$ molecule. This was found to have a significant effect on the overall computed barrier, possibly as it interrupts any intramolecular $N{-}H^{\delta+}{\cdots}H^{\delta-}{-}B$ interactions within the **$[1\text{-}H_3B{\cdot}NMeH_2]^+$** cation. This can be seen in the computed structure of the **$[1\text{-}H_3B{\cdot}NMeH_2]^+{\cdot}H_3B{\cdot}NMeH_2$** adduct (Figure 5B) where the Ir-bound amine-borane is tilted away from the N−H of the pincer ligand rather than toward it as in the molecular structure of **$[1\text{-}H_3B{\cdot}NMe_3]^+$** (Figure 2). This model is also justified by a free energy change of −1.7 kcal/mol for the formation of the

Table 3. Initial Rates for H_2 Evolution from Initial Rate Measurements and Polymer Characterization[a]

entry	catalyst	k_{obs} (×10^{-4} M/s)	M_n[b] (g/mol)	% conversion.[c] (% yield)
1	$[1\text{-}H_3B{\cdot}NMe_3]^+$	6(2)	39,900	99(60)
2	$[1\text{-}H_4]^+$[d]	7.1(8)	35,100	99(79)
3	$[1\text{-}NMeH_2]^+$	0.9(1)	49,300	99(54)
4	$[1\text{-}H_3B{\cdot}NMe_3]^+/NMeH_2$[e]	0.9(1)	48,500	84(48)
5	$[1\text{-}H_3B{\cdot}NMe_3]^+/[NMeH_3]^+$[f]	8.1(3)	15,800	97(54)
6	$[1\text{-}H_3B{\cdot}NMe]^+$/recharged[g]	0.5(2)	41,600	97[g]

[a]1 mol % cat., 0.223 M $H_3B{\cdot}NMeH_2$ (50 mg), jacketed-Schlenk flask at 293 K, 1,2-$F_2C_6H_4$ (5 mL). [b]GPC relative to polystyrene standards. [c]Measured using ^{11}B NMR spectroscopy by sampling the reaction mixture, % yield of the isolated polymer. [d]**1-H_3** made in situ. [e]2 equiv. additive to [Ir]. [f]2 equiv. relative to [Ir]. $Đ$ is between 1.5 and 1.8 for all samples. [g]Recharged with 50 mg of $H_3B{\cdot}NMeH_2$; final isolated yield not determined.

https://doi.org/10.1021/acscatal.2c03778
ACS Catal. 2022, 12, 13050−13064

Scheme 10. Proposed Catalytic Cycle and Off-Cycle Processes, for Dehydropolymerization of $H_3B{\cdot}NMeH_2$[a]

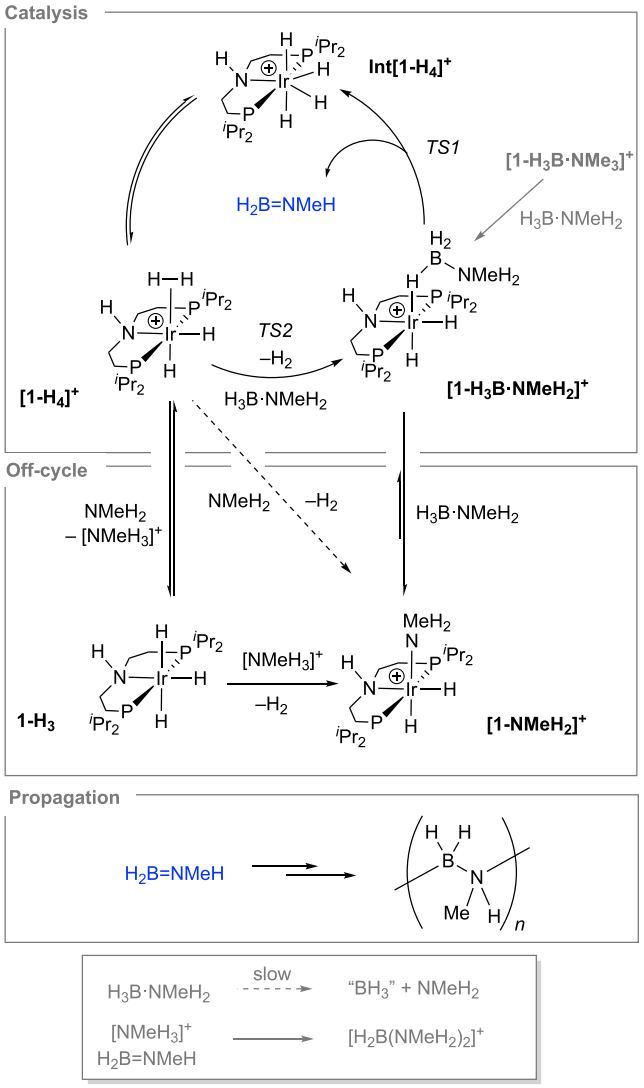

[a] $[BAr^F_4]^-$ anions and outer-sphere $H_3B{\cdot}NMeH_2$ (see text) not shown.

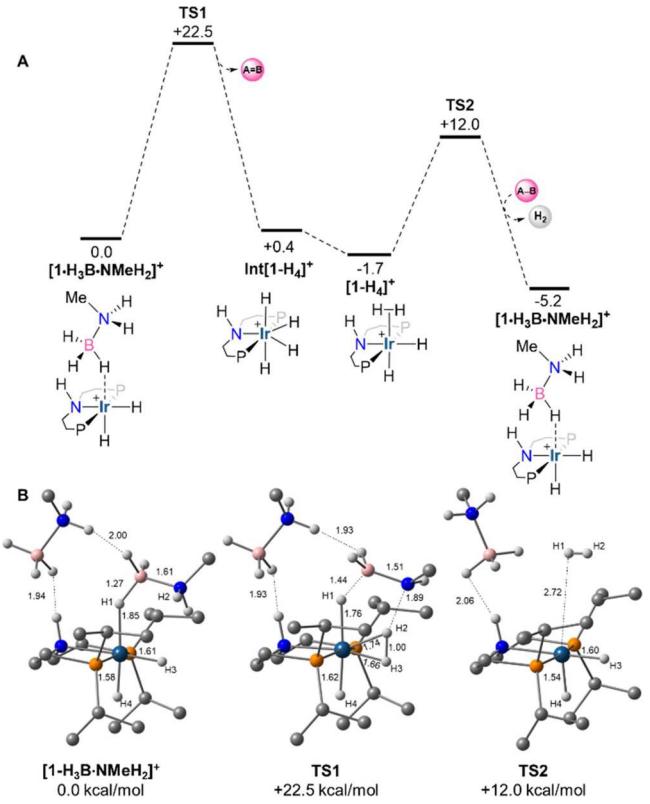

Figure 5. (A) Computed free energy profile (kcal/mol) for amine-borane dehydrogenation from $[\mathbf{1\text{-}H_3B{\cdot}NMeH_2}]^+$ (P = P^iPr_2, **MA** = methylamine, **A−B** = $H_3B{\cdot}NMeH_2$; **A═B** = H_2BNMeH; an outer-sphere $H_3B{\cdot}NMeH_2$ is always present in the computed structures but is omitted from the schematic representations for simplicity). (B) Computed structures of **A** and **TS1** and **TS2** highlighting key distances (Å) and shortest contacts to the outer-sphere $H_3B{\cdot}NMeH_2$ molecule; C−H hydrogens are omitted for clarity. Key: Ir: blue; H: white; B: pink; C: gray; N: azure; P: orange. Level of theory: BP86[D3BJ,2-hexanone][93]/Def2TZVP//BP86/SDD (Ir, P, with polarization on P); 6-31G** on all other atoms.

adduct from $[\mathbf{1\text{-}H_3B{\cdot}NMeH_2}]^+$ and free $H_3B{\cdot}NMeH_2$. The importance of including outer-sphere interactions with the ^{i}Pr-PN^{H}P ligand has recently been pointed out when modeling Ru-catalyzed formic acid dehydrogenation.[57]

A range of mechanisms were assessed for $H_3B{\cdot}NMeH_2$ dehydrogenation, and the lowest energy process is shown in Figure 5A with computed structures in Figure 5B.[94] From $[\mathbf{1\text{-}H_3B{\cdot}NMeH_2}]^+$, N−H/B−H activation proceeds in a single step via **TS1** at 22.5 kcal/mol. N−H bond cleavage is more advanced in this transition state (N···H2 = 1.89 Å; B···H1 = 1.44 Å), and proton transfer to the metal is assisted by the adjacent hydride forming an η^2-H_2 moiety (H2−H3 = 1.00 Å). Throughout the nascent aminoborane maintains N−$H^{\delta+}$···$H^{\delta-}$−B interactions with the outer-sphere $H_3B{\cdot}NMeH_2$ molecule. **TS1** leads to the formation of the tetrahydride $\mathbf{Int[1\text{-}H_4]}^+$ from which the reductive coupling of H1 and H2 to give $[\mathbf{1\text{-}H_4}]^+$ is essentially barrierless (see Scheme 6[70]). H_2 dissociation from $[\mathbf{1\text{-}H_4}]^+$ proceeds via **TS2** at +12.0 kcal/mol and in the presence of the outer-sphere $H_3B{\cdot}NMeH_2$ reforms $[\mathbf{1\text{-}H_3B{\cdot}NMeH_2}]^+$ directly to complete the catalytic cycle. The overall barrier for dehydrogenation is 22.5 kcal/mol, with the rate-limiting transition state associated with an asynchronous, concerted N−H/B−H activation step. Without the outer-sphere $H_3B{\cdot}NMeH_2$ molecule, the computed barrier is 27.5 kcal/mol, similar to previous calculations where N−H activation processes at cationic group 9 amine-boryls report rate-limiting barriers of ∼24−27 kcal/mol.[43,66] An alternative inner-sphere mechanism featuring stepwise B−H then N−H activation had a slightly higher barrier of 23.6 kcal/mol (see Supporting Materials). The displacement of $H_3B{\cdot}NMeH_2$ by $NMeH_2$ is also computed to be thermodynamically favored (ΔG = −2.8 kcal/mol), consistent with the formation of this species toward the end of the catalytic runs and the slowing of catalysis as this species becomes more prevalent.

The off-cycle processes in Scheme 10 imply a competition in the fate of $[\mathbf{1\text{-}H_4}]^+$: deprotonation to form off-cycle $\mathbf{1\text{-}H_3}$ and $[H_2B(NMeH_2)_2]^+$, or H_2 substitution to reform either $[\mathbf{1\text{-}H_3B{\cdot}NMeH_2}]^+$ or $[\mathbf{1\text{-}NMeH_2}]^+$. While the latter processes are thermodynamically favored (by 5.7 kcal/mol and 4.8 kcal/mol respectively), the deprotonation is more accessible kinetically, with a barrier (relative to $[\mathbf{1\text{-}H_4}]^+$) of 7.3 kcal/mol cf. 13.7 kcal/mol for H_2 loss (see Figures 5A and S68 for details).

In contrast to the inner-sphere process characterized here for the cationic system, the computed mechanism for the

https://doi.org/10.1021/acscatal.2c03778
ACS Catal. 2022, 12, 13050−13064

dehydrogenation of $H_3B{\cdot}NMeH_2$ by neutral **1-H$_3$** proceeds via an outer-sphere pathway analogous to that reported previously for its Rh congener (see Figure S67). This entails an overall barrier of 24.3 kcal/mol, significantly higher than that for Rh (19.7 kcal/mol) consistent with the far greater activity of the latter. Comparison of the computed profiles suggests that the higher barrier for Ir results from the stronger η^2-H_2 adduct that is formed prior to rate-limiting H_2 loss. The barrier associated with **1-H$_3$** is also 1.8 kcal/mol higher than that computed for $[\mathbf{1\text{-}H_3B{\cdot}NMeH_2}]^+$, consistent with the greater activity of the latter.

2.11. Synthesis of [Ir(^{i}Pr-PN^{Me}P)(H)$_2$(H$_3$B·NMe$_3$)][BAr$^F_4$] and Use in Catalysis: Support for the Inner-Sphere Mechanism. To rule out a ligand cooperative mechanism that involves the N−H group of the ^{i}Pr-PN^{H}P-ligand, the complex [Ir(^{i}Pr-PN^{Me}P)(H)$_2$(H$_3$B·NMe$_3$)][BAr$^F_4$], [**2-H$_3$B·NMe$_3$**][**BAr$^F_4$**], was synthesized in an analogous way to [**1-H$_3$B·NMe$_3$**][**BAr$^F_4$**], Figure 6. Hydrogenation of [Ir(^{i}Pr-PN^{Me}P)(H)$_2$(COD)][BAr$^F_4$], [**2-COD**][**BAr$^F_4$**], results in the formation of the dihydrogen/dihydride complex [**2-H$_4$**][**BAr$^F_4$**] which displays very similar NMR data to [**1-H$_4$**][**BAr$^F_4$**], that is, a single hydride resonance at 298 K that integrates to 4H (δ −10.65, T_1 = 242(2) ms), and resolves into two signals at 183 K (δ −4.87, −16.55). Addition of H$_3$B·NMe$_3$ to in situ formed [**2-H$_4$**][**BAr$^F_4$**] afforded [**2-H$_3$B·NMe$_3$**][**BAr$^F_4$**], which was characterized by NMR spectroscopy and single-crystal X-ray diffraction; with all data being very similar to [**1-H$_3$B·NMe$_3$**][**BAr$^F_4$**]. There is a small amount of recalcitrant [**2-H$_4$**][**BAr$^F_4$**] that cocrystallizes with [**2-H$_3$B·NMe$_3$**][**BAr$^F_4$**] (~10% by NMR spectroscopy). As both complexes are likely to offer the same operationally unsaturated[95] {Ir(^{i}Pr-PN^{Me}P)(H)$_2$}$^+$ fragment, this mixture was used going forward in catalytic studies.

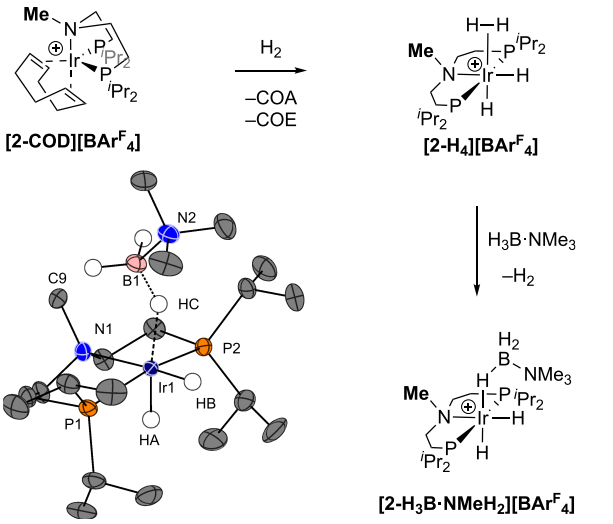

Figure 6. Synthesis of [Ir(^{i}Pr-PN^{Me}P)(H)$_2$(H$_3$B·NMe$_3$)][BAr$^F_4$] and single-crystal X-ray diffraction structure of the cation (50% displacement ellipsoids, see Supporting Materials).

When [**2-H$_3$B·NMe$_3$**][**BAr$^F_4$**] (1 mol %, 1,2-F$_2$C$_6$H$_4$) was used as a catalyst, there was relatively fast turnover, with one equivalent of H_2 released in 55 min, in contrast to [**1-H$_3$B·NMe$_3$**][**BAr$^F_4$**] (ca. 400 min). This supports an inner-sphere non-ligand-cooperative mechanism. Figure 7 compares the temporal profiles for H_2 evolution for the two catalysts, while the inset B shows that for [**2-H$_3$B·NMe$_3$**][**BAr$^F_4$**] H_2 evolution

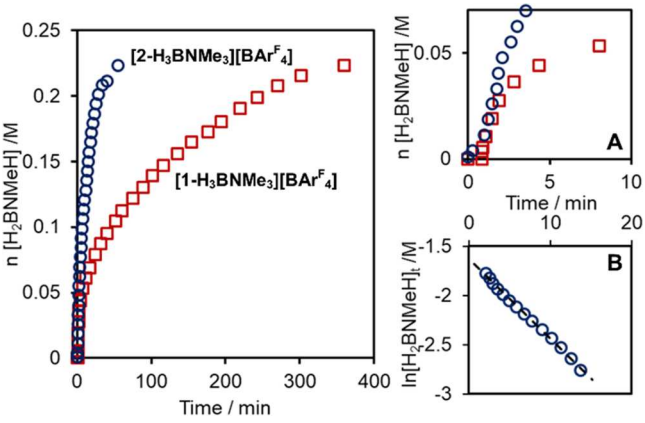

Figure 7. Temporal profiles using the two catalysts and a first-order analysis using catalyst [**2-H$_3$B·NMe$_3$**][**BAr$^F_4$**]. H$_2$B═NMeH equivalents formed from H_2 evolution (eudiometer). (A) Expansion showing the early stages of catalysis; (B) First order analysis of H_2 evolution using [**2-H$_3$B·NMe$_3$**][**BAr$^F_4$**].

occurs with overall pseudo first-order kinetics (k_{obs} = 14(2) ×10^{-4} M/s) over ~2 half-lives—in contrast to the more complex situation for [**1-H$_3$B·NMe$_3$**][**BAr$^F_4$**]. However, initial rate measurements show that both catalysts turnover at essentially the same rate [6.4(8) ×10^{-4} M/s]. This shows that the deceleratory processes occurring for [**1-H$_3$B·NMe$_3$**][**BAr$^F_4$**] are not occurring for the ^{i}Pr-PN^{Me}P analogue, at least in the early stages of catalysis. Speciation experiments after 10 min turnover show at least three complexes, two of which are spectroscopically identified as [Ir(^{i}Pr-PN^{Me}P)(H)$_2$(H$_3$B·NMe$_3$)][BAr$^F_4$], and the neutral trihydride Ir(^{i}Pr-PN^{Me}P)H$_3$, **2-H$_3$**.[96] A further as yet unidentified complex is observed [δ_P 59.3; $\delta_{(H\text{-hydride})}$ −22.49 and −22.99 ppm]. As the observation of **2-H$_3$** demonstrates that deprotonation of [**2-H$_4$**][**BAr$^F_4$**] occurs, why then are the kinetics so different?

2.12. Suggested Role of Polymer Precipitation on Observed Reaction Kinetics and Resulting Polymer Products. While we cannot discount that **2-H$_3$** is itself a competent catalyst, this is unlikely given the inactivity of **1-H$_3$** at 298 K and that Ru(^{i}Pr-PN^{Me}P) complexes are calculated to have significantly higher barriers to amine-borane dehydrogenation than their Ru(^{i}Pr-PN(*H*)P) analogues.[16] Instead, we hypothesize that reprotonation of **1-H$_3$** by [H$_2$B(NMeH$_2$)$_2$][BAr$^F_4$] or [NMeH$_3$][BAr$^F_4$] is attenuated by entrainment of these proton sources in the precipitated polymer, which results in the deceleration observed. If entrainment occurs to a significantly lesser degree for **2-H$_3$**, faster turnover would result. Such effects will be amplified by any additional coentrainment of the cationic catalyst in the precipitated polymer that reduces $[Ir]_{TOT}$. Support for this hypothesis comes from a number of observations and experiments.

(i) In comparison to [**1-H$_3$B·NMe$_3$**][**BAr$^F_4$**], catalyst [**2-H$_3$B·NMe$_3$**][**BAr$^F_4$**] is less selective, producing shorter, ill-defined, polyaminoboranes and *N*-trismethylborazine, among other B-containing oligomers, as shown by ^{11}B NMR spectroscopy (Figure 8A,B) and GPC analysis. These shorter polymers/oligomers are more soluble in 1,2-F$_2$C$_6$H$_4$, and we propose that the [H$_2$B(NMeH$_2$)$_2$][BAr$^F_4$], or [NMeH$_3$][BAr$^F_4$], that is formed is thus entrained to a lesser extent. As these also act as chain control agents, the rate of termination now becomes competitive with dehydrogenation/propagation and soluble oligomers of lower molecular

https://doi.org/10.1021/acscatal.2c03778
ACS Catal. 2022, 12, 13050−13064

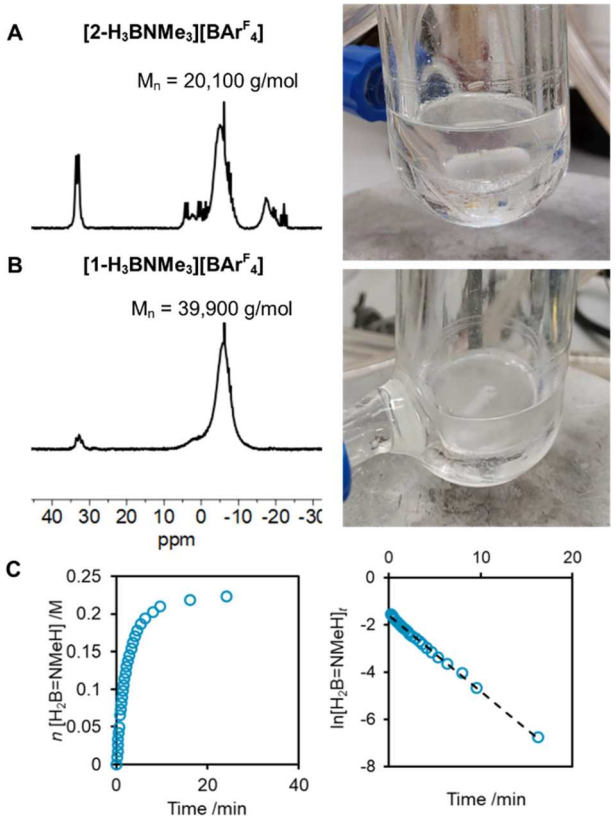

Figure 8. ^{11}B NMR spectrum and photograph of the final reaction mixture using (A) [**2-H$_3$B·NMe$_3$**][**BAr$^F_4$**] and (B) [**1-H$_3$B·NMe$_3$**][**BAr$^F_4$**]. (C) Temporal profile and first-order kinetics for [**1-H$_3$B·NMe$_3$**][**BAr$^F_4$**] (1 mol %, 10 equiv [NMeH$_3$][BAr$^F_4$]). H$_2$B═NMeH equivalents from H$_2$ evolution (eudiometer).

weight result. We suggest that the likely more nucleophilic Ir(^{i}Pr-PN^{Me}P)H$_3$, **2-H$_3$**, may also act as a more efficient initiator[12] for polymer growth, leading to shorter chains being formed. ^{i}Pr-PN^{Me}P has been shown to be a better N-donor ligand than ^{i}Pr-PN^{H}P on the basis of CO stretching frequencies in Ru-carbonyl complexes.[57,59]

(ii) Adding two equivalents of [NMeH$_3$][BAr$^F_4$] to catalysis using [**1-H$_3$B·NMe$_3$**][**BAr$^F_4$**] results in a reduction in the degree of polymerization (M_n = 15,800 g/mol). Although precipitation still occurs, GPC analysis of the isolated polymer shows significantly more [BAr$^F_4$]$^-$ is present (Supporting Materials). Notably the time-course plot for H$_2$ evolution shows a more pronounced first-order region at the start of catalysis, similar to that for [**2-H$_3$B·NMe$_3$**][**BAr$^F_4$**]. In contrast, addition of [NMeH$_3$][BAr$^F_4$] to preformed polymer (M_n = 92,400 g/mol) and work up does not result in an increase in the [BAr$^F_4$]$^-$ signal in the resulting GPC chromatogram. Using [BAr$^F_4$]$^-$ as a spectroscopic proxy for [NMeH$_3$]$^+$ thus supports its entrainment during active polymer chain growth.

(iii) Given that [NMeH$_3$]$^+$, or boronium, acts as a chain control agent and to protonate **1-H$_3$**, further increasing its ratio relative to [Ir]$_{TOT}$ should produce even shorter, more soluble oligomers, stop precipitation, and provide simpler kinetics as more catalysts will sit on-cycle. This is the case, and using 10 equivalents results in oligomers (M_n < 5000 g/mol),[97] and first-order behavior (k_{obs} = 53.7(6) ×10^{-4} M/s) being measured over at least 7 half-lives when using [**1-H$_3$B·NMe$_3$**][**BAr$^F_4$**] (1 mol %), Figure 8C. The initial rate measured also showed a significant increase in the rate of turnover, 17.8(1) ×10^{-4} M/s. Speciation using ^{31}P{^{1}H} NMR spectroscopy at ∼75% conversion (4 min) shows at least five complexes by multiple signals observed in the range δ_P of 57−51. We assign these to cationic [Ir(^{i}Pr-PN^{H}P)(H)$_2$(L)][BAr$^F_4$] species, being very similar to those observed in the early stages of catalysis using undoped [**1-H$_3$B·NMe$_3$**][**BAr$^F_4$**], cf. Figure 4.

(iv) Finally, entrainment of the [NMeH$_3$]$^+$/boronium/cationic catalyst may be expected to have a disproportionally greater effect at lower catalyst concentrations, assuming that the degree of polymer precipitation is unchanged. When compared with off-cycle neutral **1-H$_3$**, proportionally more of these cationic species would likely be entrained in the precipitated polymer, with the result that turnover slows—as is observed at 0.5 mol % (Figure 3).

3. CONCLUSIONS

In this contribution, we demonstrate that the mechansim of amine-borane dehydropolymerization continues to offer unexpected and nuanced differences depending on the choice of metal/ligand fragment.[2,3] While the perceived wisdom would be that neutral precatalysts such as **1-H$_3$**, that offer MLC mechanistic pathways, would be effective catalysts for amine-borane dehydrogenation, we show here that they are not fully consistent with Fagnou's very brief observation nearly 15 years ago on related systems.[62] That the cationic catalyst manifold offers a lower energy pathway and produces polymer selectively (albeit at 1 mol % catalyst loading) via a non-MLC route was also initially surprising.[25,27,49,52] Moreover, the role of NMeH$_2$, formed from slow B−N bond cleavage, is different from other recently reported systems. Here, it has an inhibitory role, by promoting the formation **1-H$_3$**, in contrast to other systems where its role is accelatory by bringing a cationic precatalyst onto the catalytic cycle through promoting hydride transfer to form an active, neutral, catalyst. Finally, and perhaps a more obvious comment, is that significant caution needs to be excercised in interpreting kinetic data when polyaminoborane precipitates from solution, due to the possibility of entrainment of coproducts or catalyst in the catalytic manifold. Moving forward, while the systems under discussion here do not match the efficency of other catalysts in terms of ToF or ToN,[16,19,25,52] the ability to switch on productive catalytic turnover by simple addition of [NMeH$_3$][BAr$^F_4$] to **1-H$_3$** offers the possibility for temporally and spatially controlled dehydropolymerization[98] catalysis that may offer benefits in both H$_2$ release profiles and the resulting material properties

■ ASSOCIATED CONTENT

Supporting Information

The Supporting Information is available free of charge at https://pubs.acs.org/doi/10.1021/acscatal.2c03778.

Full details of experimental and characterization data for the new complexes, kinetics data, and computational studies (PDF)

Coordinates of computed intermediates and transition states (XYZ)

Accession Codes

CCDC 2172743−2172745 and 2183097, 2183098 contain the supplementary crystallographic data for this paper. These data can be obtained free of charge via www.ccdc.cam.ac.uk/data_request/cif, or by emailing data_request@ccdc.cam.ac.uk, or by contacting The Cambridge Crystallographic Data Centre,

https://doi.org/10.1021/acscatal.2c03778
ACS Catal. 2022, 12, 13050−13064

12 Union Road, Cambridge CB2 1EZ, UK; fax: +441,223 336,033.

AUTHOR INFORMATION

Corresponding Authors

Claire N. Brodie − *Department of Chemistry, University of York, York YO10 5DD, U.K.;* orcid.org/0000-0002-8896-0270; Email: claire.brodie@york.ac.uk

Stuart A. Macgregor − *Institute of Chemical Sciences, Heriot-Watt University, Edinburgh EH14 4AS, U.K.;* orcid.org/0000-0003-3454-6776; Email: S.A.Macgregor@hw.ac.uk

Andrew S. Weller − *Department of Chemistry, University of York, York YO10 5DD, U.K.;* orcid.org/0000-0003-1646-8081; Email: andrew.weller@york.ac.uk

Authors

Lia Sotorrios − *Institute of Chemical Sciences, Heriot-Watt University, Edinburgh EH14 4AS, U.K.;* orcid.org/0000-0002-2956-8092

Timothy M. Boyd − *Department of Chemistry, University of York, York YO10 5DD, U.K.; Chemistry Research Laboratories, University of Oxford, Oxford OX1 3TA, U.K.*

Complete contact information is available at: https://pubs.acs.org/10.1021/acscatal.2c03778

Author Contributions

The manuscript was written through contributions of all authors.

Funding

EPSRC (EP/M024210/2, EP/T019867/1, DTP to TMB), The University of York via the EPSRC Impact Acceleration Account.

Notes

The authors declare no competing financial interest.

ACKNOWLEDGMENTS

The EPSRC, University of York, for funding. Mathew Cross (University of York) is acknowledged for experimental assistance with re-charging experiments. The referees are thanked for insightful and useful comments.

REFERENCES

(1) Staubitz, A.; Soto, A. P.; Manners, I. Iridium-Catalyzed Dehydrocoupling of Primary Amine-Borane Adducts: A Route to High Molecular Weight Polyaminoboranes, Boron-Nitrogen Analogues of Polyolefins. *Angew. Chem., Int. Ed.* **2008**, *47*, 6212−6215.

(2) Colebatch, A. L.; Weller, A. S. Amine−Borane Dehydropolymerization: Challenges and Opportunities. *Chem. −Eur. J.* **2019**, *25*, 1379−1390.

(3) Han, D.; Anke, F.; Trose, M.; Beweries, T. Recent Advances in Transition Metal Catalysed Dehydropolymerisation of Amine Boranes and Phosphine Boranes. *Coord. Chem. Rev.* **2019**, *380*, 260−286.

(4) Johnson, H. C.; Hooper, T. N.; Weller, A. S. The Catalytic Dehydrocoupling of Amine−Boranes and Phosphine−Boranes. *Top. Organomet. Chem.* **2015**, *49*, 153.

(5) Staubitz, A.; Sloan, M. E.; Robertson, A. P. M.; Friedrich, A.; Schneider, S.; Gates, P. J.; Schmedt auf der Günne, J.; Manners, I. Catalytic Dehydrocoupling/Dehydrogenation of *N*-Methylamine-Borane and Ammonia-Borane: Synthesis and Characterization of High Molecular Weight Polyaminoboranes. *J. Am. Chem. Soc.* **2010**, *132*, 13332−13345.

(6) Priegert, A. M.; Rawe, B. W.; Serin, S. C.; Gates, D. P. Polymers and the P-Block Elements. *Chem. Soc. Rev.* **2016**, *45*, 922−953.

(7) Rossin, A.; Peruzzini, M. Ammonia-Borane and Amine-Borane Dehydrogenation Mediated by Complex Metal Hydrides. *Chem. Rev.* **2016**, *116*, 8848−8872.

(8) Vidal, F.; Jäkle, F. Functional Polymeric Materials Based on Main-Group Elements. *Angew. Chem., Int. Ed.* **2019**, *58*, 5846−5870.

(9) Peterson, G. I.; Choi, T.-L. Cascade Polymerizations: Recent Developments in the Formation of Polymer Repeat Units by Cascade Reactions. *Chem. Sci.* **2020**, *11*, 4843−4854.

(10) Metters, O. J.; Chapman, A. M.; Robertson, A. P. M.; Woodall, C. H.; Gates, P. J.; Wass, D. F.; Manners, I. Generation of Aminoborane Monomers RR′N═BH_2 from Amine−Boronium Cations $[RR'NH{-}BH_2L]^+$: Metal Catalyst-Free Formation of Polyaminoboranes at Ambient Temperature. *Chem. Commun.* **2014**, *50*, 12146−12149.

(11) Pons, V.; Baker, R. T.; Szymczak, N. K.; Heldebrant, D. J.; Linehan, J. C.; Matus, M. H.; Grant, D. J.; Dixon, D. A. Coordination of Aminoborane, NH_2BH_2, Dictates Selectivity and Extent of H_2 Release in Metal-Catalysed Ammonia Borane Dehydrogenation. *Chem. Commun.* **2008**, *48*, 6597−6599.

(12) Bhunya, S.; Malakar, T.; Paul, A. Unfolding the Crucial Role of a Nucleophile in Ziegler−Natta Type Ir Catalyzed Polyaminoborane Formation. *Chem. Commun.* **2014**, *50*, 5919−5922.

(13) Ganguly, G.; Malakar, T.; Paul, A. Theoretical Studies on the Mechanism of Homogeneous Catalytic Olefin Hydrogenation and Amine-Borane Dehydrogenation by a Versatile Boryl-Ligand-Based Cobalt Catalyst. *ACS Catal.* **2015**, *5*, 2754−2769.

(14) Marquardt, C.; Jurca, T.; Schwan, K. C.; Stauber, A.; Virovets, A. V.; Whittell, G. R.; Manners, I.; Scheer, M. Metal-Free Addition/Head-to-Tail Polymerization of Transient Phosphinoboranes, RPH-BH_2: A Route to Poly(Alkylphosphinoboranes). *Angew. Chem., Int. Ed.* **2015**, *54*, 13782−13786.

(15) Johnson, H. C.; Robertson, A. P. M.; Chaplin, A. B.; Sewell, L. J.; Thompson, A. L.; Haddow, M. F.; Manners, I.; Weller, A. S. Catching the First Oligomerization Event in the Catalytic Formation of Polyaminoboranes: $H_3B{\cdot}NMeHBH_2{\cdot}NMeH_2$ Bound to Iridium. *J. Am. Chem. Soc.* **2011**, *133*, 11076−11079.

(16) Marziale, A. N.; Friedrich, A.; Klopsch, I.; Drees, M.; Celinski, V. R.; Schmedt Auf Der Günne, J.; Schneider, S. The Mechanism of Borane-Amine Dehydrocoupling with Bifunctional Ruthenium Catalysts. *J. Am. Chem. Soc.* **2013**, *135*, 13342−13355.

(17) Anke, F.; Han, D.; Klahn, M.; Spannenberg, A.; Beweries, T. Formation of High-Molecular Weight Polyaminoborane by Fe Hydride Catalysed Dehydrocoupling of Methylamine Borane. *Dalton Trans.* **2017**, *46*, 6843−6847.

(18) Anke, F.; Boye, S.; Spannenberg, A.; Lederer, A.; Heller, D.; Beweries, T. Dehydropolymerisation of Methylamine Borane and an *N*-Substituted Primary Amine Borane Using a PNP Fe Catalyst. *Chem. − Eur. J.* **2020**, *26*, 7889−7899.

(19) Glüer, A.; Förster, M.; Celinski, V. R.; Schmedt Auf Der Günne, J.; Holthausen, M. C.; Schneider, S. Highly Active Iron Catalyst for Ammonia Borane Dehydrocoupling at Room Temperature. *ACS Catal.* **2015**, *5*, 7214−7217.

(20) Boyd, T. M.; Andrea, K. A.; Baston, K.; Johnson, A.; Ryan, D. E.; Weller, A. S. A Simple Cobalt-Based Catalyst System for the Controlled Dehydropolymerisation of $H_3B{\cdot}NMeH_2$ on the Gram-Scale. *Chem. Commun.* **2020**, *56*, 482−485.

(21) Maier, T. M.; Sandl, S.; Shenderovich, I. G.; Jacobi von Wangelin, A.; Weigand, J. J.; Wolf, R. Amine-Borane Dehydrogenation and Transfer Hydrogenation Catalyzed by α-Diimine Cobaltates. *Chem. − Eur. J.* **2019**, *25*, 238−245.

(22) Todisco, S.; Luconi, L.; Giambastiani, G.; Rossin, A.; Peruzzini, M.; Golub, I. E.; Filippov, O. A.; Belkova, N. V.; Shubina, E. S. Ammonia Borane Dehydrogenation Catalyzed by $(\kappa^4\text{-}EP_3)Co(H)$ $[EP_3 = E(CH_2CH_2PPh_2)_3$; E = N, P] and H_2 Evolution from Their Interaction with NH Acids. *Inorg. Chem.* **2017**, *56*, 4296−4307.

(23) Pagano, J. K.; Stelmach, J. P. W.; Waterman, R. Cobalt-Catalyzed Ammonia Borane Dehydrocoupling and Transfer Hydrogenation under Aerobic Conditions. *Dalton Trans.* **2015**, *44*, 12074−12077.

(24) Colebatch, A. L.; Hawkey Gilder, B. W.; Whittell, G. R.; Oldroyd, N. L.; Manners, I.; Weller, A. S. A General, Rhodium-Catalyzed, Synthesis of Deuterated Boranes and *N*-Methyl Polyaminoboranes. *Chem. – Eur. J.* **2018**, *24*, 5450−5455.
(25) Adams, G. M.; Colebatch, A. L.; Skornia, J. T.; McKay, A. I.; Johnson, H. C.; Lloyd-Jones, G. C.; Macgregor, S. A.; Beattie, N. A.; Weller, A. S. Dehydropolymerization of $H_3B{\cdot}NMeH_2$ to Form Polyaminoboranes Using [Rh(Xantphos-Alkyl)] Catalysts. *J. Am. Chem. Soc.* **2018**, *140*, 1481−1495.
(26) Hasche, P.; Haak, J.; Anke, F.; Kubis, C.; Baumann, W.; Drexler, H. J.; Jiao, H.; Beweries, T. Dehydropolymerisation of Methylamine Borane Using Highly Active Rhodium(III) Bis-(Thiophosphinite) Pincer Complexes: Catalytic and Mechanistic Insights. *Catal. Sci. Technol.* **2021**, *11*, 3514−3526.
(27) Ryan, D. E.; Andrea, K. A.; Race, J. J.; Boyd, T. M.; Lloyd-Jones, G. C.; Weller, A. S. Amine-Borane Dehydropolymerization Using Rh-Based Precatalysts: Resting State, Chain Control, and Efficient Polymer Synthesis. *ACS Catal.* **2020**, *10*, 7443−7448.
(28) Adams, G. M.; Ryan, D. E.; Beattie, N. A.; McKay, A. I.; Lloyd-Jones, G. C.; Weller, A. S. Dehydropolymerization of $H_3B{\cdot}NMeH_2$ Using a $[Rh(DPEphos)]^+$ Catalyst: The Promoting Effect of $NMeH_2$. *ACS Catal.* **2019**, *9*, 3657−3666.
(29) Johnson, H. C.; Leitao, E. M.; Whittell, G. R.; Manners, I.; Lloyd-Jones, G. C.; Weller, A. S. Mechanistic Studies of the Dehydrocoupling and Dehydropolymerization of Amine-Boranes Using a $[Rh(Xantphos)]^+$ Catalyst. *J. Am. Chem. Soc.* **2014**, *136*, 9078−9093.
(30) Trose, M.; Reiß, M.; Reiß, F.; Anke, F.; Spannenberg, A.; Boye, S.; Lederer, A.; Arndt, P.; Beweries, T. Dehydropolymerisation of Methylamine Borane Using a Dinuclear 1,3-Allenediyl Bridged Zirconocene Complex. *Dalton Trans.* **2018**, *47*, 12858−12862.
(31) Lapierre, E. A.; Patrick, B. O.; Manners, I. Trivalent Titanocene Alkyls and Hydrides as Well-Defined, Highly Active, and Broad Scope Precatalysts for Dehydropolymerization of Amine-Boranes. *J. Am. Chem. Soc.* **2019**, *141*, 20009−20015.
(32) Jurca, T.; Dellermann, T.; Stubbs, N. E.; Resendiz-Lara, D. A.; Whittell, G. R.; Manners, I. Step-Growth Titanium-Catalysed Dehydropolymerisation of Amine-Boranes. *Chem. Sci.* **2018**, *9*, 3360−3366.
(33) *Smart Inorganic Polymers*; Hey-Hawkins, E.; Hissler, M., Eds.; Wiley-VCH: Weinheim, 2019.
(34) Zhang, Y.; Hopkins, M. A.; Liptrot, D. J.; Khanbareh, H.; Groen, P.; Zhou, X.; Zhang, D.; Bao, Y.; Zhou, K.; Bowen, C. R.; Carbery, D. R. Harnessing Plasticity in an Amine-Borane as a Piezoelectric and Pyroelectric Flexible Film. *Angew. Chem., Int. Ed.* **2020**, *59*, 7808−7812.
(35) Leitao, E. M.; Jurca, T.; Manners, I. Catalysis in Service of Main Group Chemistry Offers a Versatile Approach to P-Block Molecules and Materials. *Nat. Chem.* **2013**, *5*, 817−829.
(36) Resendiz-Lara, D. A.; Whittell, G. R.; Leitao, E. M.; Manners, I. Catalytic Synthesis, Characterization, and Properties of Polyaminoborane Homopolymers and Random Copolymers. *Macromolecules* **2019**, *52*, 7052−7064.
(37) Wang, X.; Hooper, T. N.; Kumar, A.; Priest, I. K.; Sheng, Y.; Samuels, T. O. M.; Wang, S.; Robertson, A. W.; Pacios, M.; Bhaskaran, H.; Weller, A. S.; Warner, J. H. Oligomeric Aminoborane Precursors for the Chemical Vapour Deposition Growth of Few-Layer Hexagonal Boron Nitride. *CrystEngComm* **2017**, *19*, 285−294.
(38) Bernard, S.; Miele, P. Polymer-Derived Boron Nitride: A Review on the Chemistry, Shaping and Ceramic Conversion of Borazine Derivatives. *Materials* **2014**, *7*, 7436−7459.
(39) Du, V. A.; Jurca, T.; Whittell, G. R.; Manners, I. Aluminum Borate Nanowires from the Pyrolysis of Polyaminoborane Precursors. *Dalton Trans.* **2016**, *45*, 1055−1062.
(40) Baker, R. T.; Gordon, J. C.; Hamilton, C. W.; Henson, N. J.; Lin, P. H.; Maguire, S.; Murugesu, M.; Scott, B. L.; Smythe, N. C. Iron Complex-Catalyzed Ammonia-Borane Dehydrogenation. A Potential Route toward B-N-Containing Polymer Motifs Using Earth-Abundant Metal Catalysts. *J. Am. Chem. Soc.* **2012**, *134*, 5598−5609.
(41) Devillard, M.; De Albuquerque Pinheiro, C. A.; Caytan, E.; Roiland, C.; Dinoi, C.; Del Rosal, I.; Alcaraz, G. Uncatalyzed Formation of Polyaminoboranes from Diisopropylaminoborane and Primary Amines: A Kinetically Controlled Polymerization Reaction. *Adv. Synth. Catal.* **2021**, *363*, 2417−2426.
(42) Luconi, L.; Osipova, E. S.; Giambastiani, G.; Peruzzini, M.; Rossin, A.; Belkova, N. V.; Filippov, O. A.; Titova, E. M.; Pavlov, A. A.; Shubina, E. S. Amine Boranes Dehydrogenation Mediated by an Unsymmetrical Iridium Pincer Hydride: (PCN) vs (PCP) Improved Catalytic Performance. *Organometallics* **2018**, *37*, 3142−3153.
(43) Kumar, A.; Johnson, H. C.; Hooper, T. N.; Weller, A. S.; Algarra, A. G.; Macgregor, S. A. Multiple Metal-Bound Oligomers from Ir-Catalysed Dehydropolymerisation of $H_3B{\cdot}NH_3$ as Probed by Experiment and Computation. *Chem. Sci.* **2014**, *5*, 2546−2553.
(44) Esteruelas, M. A.; López, A. M.; Mora, M.; Oñate, E. Ammonia-Borane Dehydrogenation Promoted by an Osmium Dihydride Complex: Kinetics and Mechanism. *ACS Catal.* **2015**, *5*, 187−191.
(45) Paul, A.; Musgrave, C. B. Catalyzed Dehydrogenation of Amniona-Borane by Iridium Dihydrogen Pincer Complex Differs from Ethane Dehydrogenation. *Angew. Chem., Int. Ed.* **2007**, *46*, 8153−8156.
(46) Ortega-Lepe, I.; Rossin, A.; Sánchez, P.; Santos, L. L.; Rendón, N.; Álvarez, E.; López-Serrano, J.; Suárez, A. Ammonia-Borane Dehydrogenation Catalyzed by Dual-Mode Proton-Responsive Ir-CNNH Complexes. *Inorg. Chem.* **2021**, *60*, 18490−18502.
(47) For recent reviews on MLC Process See: (a) Khusnutdinova, R.; Milstein, D. *Angew. Chem., Int. Ed.* **2015**, *42*, 12236−12273. (b) Elsby, M. R.; Baker. *Chem. Soc. Rev.* **2020**, *49*, 8933−8987. (c) Alig, L.; Fritz, M.; Schneider, C. *Chem. Rev.* **2019**, *119*, 2681−2751.
(48) Roselló-Merino, M.; López-Serrano, J.; Conejero, S. Dehydrocoupling Reactions of Dimethylamine-Borane by Pt(II) Complexes: A New Mechanism Involving Deprotonation of Boronium Cations. *J. Am. Chem. Soc.* **2013**, *135*, 10910−10913.
(49) Spearing-Ewyn, E. A. K.; Beattie, N. A.; Colebatch, A. L.; Martinez-Martinez, A. J.; Docker, A.; Boyd, T. M.; Baillie, G.; Reed, R.; Macgregor, S. A.; Weller, A. S. The Role of Neutral Rh(PONOP)-H, Free NMe_2H, Boronium and Ammonium Salts in the Dehydrocoupling of Dimethylamine-Borane Using the Cationic Pincer $[Rh(PONOP)(\eta^2\text{-}H_2)]^+$ Catalyst. *Dalton Trans.* **2019**, *48*, 14724−14736.
(50) Osipova, E. S.; Gulyaeva, E. S.; Gutsul, E. I.; Kirkina, V. A.; Pavlov, A. A.; Nelyubina, Y. V.; Rossin, A.; Peruzzini, M.; Epstein, L. M.; Belkova, N. V.; Filippov, O. A.; Shubina, E. S. Bifunctional Activation of Amine-Boranes by the W/Pd Bimetallic Analogs of "Frustrated Lewis Pairs". *Chem. Sci.* **2021**, *12*, 3682−3692.
(51) Käß, M.; Friedrich, A.; Drees, M.; Schneider, S. Ruthenium Complexes with Cooperative PNP Ligands: Bifunctional Catalysts for the Dehydrogenation of Ammonia-Borane. *Angew. Chem., Int. Ed.* **2009**, *48*, 905−907.
(52) Brodie, C. N.; Boyd, T. M.; Sotorríos, L.; Ryan, D. E.; Magee, E.; Huband, S.; Town, J. S.; Lloyd-Jones, G. C.; Haddleton, D. M.; Macgregor, S. A.; Weller, A. S. Controlled Synthesis of Well-Defined Polyaminoboranes on Scale Using a Robust and Efficient Catalyst. *J. Am. Chem. Soc.* **2021**, *143*, 21010−21023.
(53) Clarke, Z. E.; Maragh, P. T.; Dasgupta, T. P.; Gusev, D. G.; Lough, A. J.; Abdur-Rashid, K. A Family of Active Iridium Catalysts for Transfer Hydrogenation of Ketones. *Organometallics* **2006**, *25*, 4113−4117.
(54) Chen, X.; Jia, W.; Guo, R.; Graham, T. W.; Gullons, M. A.; Abdur-Rashid, K. Highly Active Iridium Catalysts for the Hydrogenation of Ketones and Aldehydes. *Dalton Trans.* **2009**, *8*, 1407−1410.
(55) Schmeier, T. J.; Dobereiner, G. E.; Crabtree, R. H.; Hazari, N. Secondary Coordination Sphere Interactions Facilitate the Insertion Step in an Iridium(III) CO_2 Reduction Catalyst. *J. Am. Chem. Soc.* **2011**, *133*, 9274−9277.

(56) Junge, K.; Wendt, B.; Jiao, H.; Beller, M. Iridium-Catalyzed Hydrogenation of Carboxylic Acid Esters. *ChemCatChem* **2014**, *6*, 2810−2814.
(57) Curley, J. B.; Hert, C.; Bernskoetter, W. H.; Hazari, N.; Mercado, B. Q. Control of Catalyst Isomers Using an *N*-Phenyl-Substituted $RN(CH_2CH_2P^iPr_2)_2$ Pincer Ligand in CO_2 Hydrogenation and Formic Acid Dehydrogenation. *Inorg. Chem.* **2022**, *61*, 643−656.
(58) Zhang, G.; Vasudevan, K. V.; Scott, B. L.; Hanson, S. K. Understanding the Mechanisms of Cobalt-Catalyzed Hydrogenation and Dehydrogenation Reactions. *J. Am. Chem. Soc.* **2013**, *135*, 8668−8681.
(59) Alberico, E.; Lennox, A. J. J.; Vogt, L. K.; Jiao, H.; Baumann, W.; Drexler, H. J.; Nielsen, M.; Spannenberg, A.; Checinski, M. P.; Junge, H.; Beller, M. Unravelling the Mechanism of Basic Aqueous Methanol Dehydrogenation Catalyzed by Ru-PNP Pincer Complexes. *J. Am. Chem. Soc.* **2016**, *138*, 14890−14904.
(60) Zhang, X.; Kam, L.; Trerise, R.; Williams, T. J. Ruthenium-Catalyzed Ammonia Borane Dehydrogenation: Mechanism and Utility. *Acc. Chem. Res.* **2017**, *50*, 86−95.
(61) Metters, O. J.; Flynn, S. R.; Dowds, C. K.; Sparkes, H. A.; Manners, I.; Wass, D. F. Catalytic Dehydrocoupling of Amine-Boranes Using Cationic Zirconium(IV)-Phosphine Frustrated Lewis Pairs. *ACS Catal.* **2016**, *6*, 6601−6611.
(62) Blaquiere, N.; Diallo-Garcia, S.; Gorelsky, S. I.; Black, D. A.; Fagnou, K. Ruthenium-Catalyzed Dehydrogenation of Ammonia Boranes. *J. Am. Chem. Soc.* **2008**, *130*, 14034−14035.
(63) Friedrich, A.; Ghosh, R.; Kolb, R.; Herdtweck, E.; Schneider, S. Iridium Olefin Complexes Bearing Dialkylamino/Amido PNP Pincer Ligands: Synthesis, Reactivity, and Solution Dynamics. *Organometallics* **2009**, *28*, 708−718.
(64) Friedrich, A.; Drees, M.; Schneider, S. Ruthenium-Catalyzed Dimethylamineborane Dehydrogenation: Stepwise Metal-Centered Dehydrocyclization. *Chem. − Eur. J.* **2009**, *15*, 10339−10342.
(65) Stephens, F. H.; Baker, R. T.; Matus, M. H.; Grant, D. J.; Dixon, D. A. Acid Initiation of Ammonia-Borane Dehydrogenation for Hydrogen Storage. *Angew. Chem., Int. Ed.* **2007**, *46*, 746−749.
(66) Douglas, T. M.; Chaplin, A. B.; Weller, A. S.; Yang, X.; Hall, M. B. Monomeric and Oligomeric Amine-Borane σ-Complexes of Rhodium. Intermediates in the Catalytic Dehydrogenation of Amine-Boranes. *J. Am. Chem. Soc.* **2009**, *131*, 15440−15456.
(67) Alcaraz, G.; Chaplin, A. B.; Stevens, C. J.; Clot, E.; Vendier, L.; Weller, A. S.; Sabo-Etienne, S. Ruthenium, Rhodium, and Iridium Bis(σ-B-H) Diisopropylaminoborane Complexes. *Organometallics* **2010**, *29*, 5591−5595.
(68) Stevens, C. J.; Dallanegra, R.; Chaplin, A. B.; Weller, A. S.; MacGregor, S. A.; Ward, B.; McKay, D.; Alcaraz, G.; Sabo-Etienne, S. $[Ir(PCy_3)_2(H)_2(H_2B\text{-}NMe_2)]^+$ as a Latent Source of Aminoborane: Probing the Role of Metal in the Dehydrocoupling of $H_3B\text{-}NMe_2H$ and Retrodimerisation of $[H_2BNMe_2]_2$. *Chem. − Eur. J.* **2011**, *17*, 3011−3020.
(69) Schiwek, C.; Meiners, J.; Förster, M.; Würtele, C.; Diefenbach, M.; Holthausen, M. C.; Schneider, S. Oxygen Reduction with a Bifunctional Iridium Dihydride Complex. *Angew. Chem., Int. Ed.* **2015**, *54*, 15271−15275.
(70) While transition states were located on the electronic surface for the formation of the tetrahydride intermediate from both the *syn* and *anti* forms of $[\mathbf{1}\text{-}\mathbf{H}_4]^+$, the inclusion of zero-point energy, thermochemical and entropy corrections suggested these would not be stationary points on the free energy surface (see Supporting Information).
(71) Wisniewski, L. L.; Zilm, K. W.; Mediati, M.; Jensen, C. M. Mechanism of Hydride Scrambling in a Transition-Metal Dihydrogen Dihydride As Studied by Solid-State Proton NMR. *J. Am. Chem. Soc.* **1993**, *115*, 7533−7534.
(72) Li, S.; Hall, M. B.; Eckert, J.; Jensen, C. M.; Albinati, A. Transition Metal Polyhydride Complexes. Intramolecular Hydrogen Exchange in the Octahedral Iridium(III) Dihydrogen Dihydride Complexes $IrXH_2(H_2\text{-}H_2)(PR_3)_2$ (X = Cl, Br, I). *J. Am. Chem. Soc.* **2000**, *122*, 2903−2910.
(73) Ingleson, M. J.; Brayshaw, S. K.; Mahon, M. F.; Ruggiero, G. D.; Weller, A. S. Dihydrogen Complexes of Rhodium: $[RhH_2(H_2)_x(PR_3)_2]^+$ (R = Cy, ^{i}Pr; x = 1, 2). *Inorg. Chem.* **2005**, *44*, 3162−3171.
(74) Hebden, T. J.; Goldberg, K. I.; Heinekey, M. D.; Zhang, X.; Emge, T. J.; Goldman, A. S.; Krogh-Jespersen, K. Dihydrogen/Dihydride or Tetrahydride? An Experimental and Computational Investigation of Pincer Iridium Polyhydrides. *Inorg. Chem.* **2010**, *49*, 1733−1742.
(75) Ledger, A. E. W.; Ellul, C. E.; Mahon, M. F.; Williams, J. M. J.; Whittlesey, M. K. Ruthenium Bidentate Phosphine Complexes for the Coordination and Catalytic Dehydrogenation of Amine- and Phosphine-Boranes. *Chem. − Eur. J.* **2011**, *17*, 8704−8713.
(76) Shimoi, M.; Nagai, S. I.; Ichikawa, M.; Kawano, Y.; Katoh, K.; Uruichi, M.; Ogino, H. Coordination Compounds of Monoborane-Lewis Base Adducts: Syntheses and Structures of $[M(CO)_5(\eta^1\text{-}BH_3\cdot L)]$ (M = Cr, Mo, W; L = NMe_3, PMe_3, PPh_3). *J. Am. Chem. Soc.* **1999**, *121*, 11704−11712.
(77) Johnson, H. C.; McMullin, C. L.; Pike, S. D.; Macgregor, S. A.; Weller, A. S. Dehydrogenative Boron Homocoupling of an Amine-Borane. *Angew. Chem., Int. Ed.* **2013**, *52*, 9776−9780.
(78) Custelcean, R.; Jackson, J. E. Dihydrogen Bonding: Structures, Energetics, and Dynamics. *Chem. Rev.* **2001**, *101*, 1963−1980.
(79) Algarra, A. G.; Sewell, L. J.; Johnson, H. C.; Macgregor, S. A.; Weller, A. S. A Combined Experimental and Computational Study of Fluxional Processes in Sigma Amine-Borane Complexes of Rhodium and Iridium. *Dalton Trans.* **2014**, *43*, 11118−11128.
(80) Significant N−H···X hydrogen bonding shifts the N−H signal downfield in the ^{1}H NMR spectrum, for example $[Rh(^iPr\text{-}PN^HP)(NBD)]Cl$ δ 6.99. Ref 52.
(81) This alternative B−H activation readily proceeds with concomitant reductive coupling of the two deuteride ligands to form $[Ir(^iPrPN^HP)(H_2B\cdot NMe_3)(H)(\eta^2\text{-}D_2)]^+$ (cf. intermediate **B** in Figure 5). However, H/D exchange then entails a transition state at +34.5 kcal/mol.
(82) 1M solutions of *N*-methylpolyaminoborane (45,000 g/mol) are visibly turbid in $1,2\text{-}F_2C_6H_4$ solvent, with significant suspended material. In THF there is only a slight haze observed in the solution, suggesting THF solvates the polymer significantly better.
(83) Increasing $[H_3B\cdot NMeH_2]$ to 1.1 M did increase the initial rate of reaction, consistent with $H_3B\cdot NMeH_2$ binding competitively with THF, but deactivation was also more significant, with only 20% conversion reached.
(84) Burés, J. Variable Time Normalization Analysis: General Graphical Elucidation of Reaction Orders from Concentration Profiles. *Angew. Chem., Int. Ed.* **2016**, *55*, 16084−16087.
(85) Lunelli, B.; Giorgini, M. G. The Vibrational Spectrum of 1, 2-Difluorobenzene and 1,2-Difluorobenzene-D_4. *J. Mol. Spectrosc.* **1977**, *64*, 1−14.
(86) Aldridge, S.; Downs, A. J.; Tang, C. Y.; Parsons, S.; Clarke, M. C.; Johnstone, R. D. L.; Robertson, H. E.; Rankin, D. W. H.; Wann, D. A. Structures and Aggregation of the Methylamine-Borane Molecules, $Me_nH_{3-n}N\cdot BH_3$ (n = 1-3), Studied by X-Ray Diffraction, Gas-Phase Electron Diffraction, and Quantum Chemical Calculations. *J. Am. Chem. Soc.* **2009**, *131*, 2231−2243.
(87) Li, J.; Kathmann, S. M.; Hu, H. S.; Schenter, G. K.; Autrey, T.; Gutowski, M. Theoretical Investigations on the Formation and Dehydrogenation Reaction Pathways of $H(NH_2BH_2)NH$ (n = 1-4) Oligomers: Importance of Dihydrogen Interactions. *Inorg. Chem.* **2010**, *49*, 7710−7720.
(88) Kubas, G. J. *Metal Dihydrogen and σ-Bond Complexes*; Kluwer: New York, 2001.
(89) Addition of $[NMe_2H_2][BAr^F_4]$ to in situ generated $H_2B{=}NMe_2$ (from retrodimerization of $[H_2BNMe_2]_2$ − see 68) forms the corresponding boronium species, $[H_2B(NMe_2H)_2][BAr^F_4]$ quantitatively. Experiments also show that $[H_2B(NMeH_2)_2][BAr^F_4]$ and

https://doi.org/10.1021/acscatal.2c03778
ACS Catal. 2022, 12, 13050−13064

$[NMe_2H_2][BAr^F{}_4]$ are interchangeable in their reaction chemistry described here.
(90) Linear transits designed to model Mechanism C resulted in high energies without passing through any maxima, suggesting there is not an accessible transition state for this process.
(91) Ríos, P.; Rodríguez, A.; Conejero, S. Activation of Si−H and B−H Bonds by Lewis Acidic Transition Metals and p-Block Elements: Same, but Different. *Chem. Sci.* **2022**, *13*, 7392−7418.
(92) Potter, R. G.; Camaioni, D. M.; Vasiliu, M.; Dixon, D. A. Thermochemistry of Lewis Adducts of BH_3 and Nucleophilic Substitution of Triethylamine on NH_3BH_3 in Tetrahydrofuran. *Inorg. Chem.* **2010**, *49*, 10512−10521.
(93) 2-Hexanone was used to mimic the dielectric constant of 1,2-$F_2C_6H_4$, the latter not being available in Gaussian 16.
(94) All attempts to define an MLC mechanism related to B, Scheme 2 were unsuccessful: linear transits exploring direct loss of H_2 via $N-H^{\delta+}\cdots{}^{\delta-}H-B$ coupling rose to high energies without passing through a maximum, while deprotonation of the ^{i}Pr-PN^{H}P proton was thermodynamically inaccessible (ΔG = +25.7 kcal/mol).
(95) Ozerov, O. V.; Watson, L. A.; Pink, M.; Caulton, K. G. Operationally Unsaturated Pincer/Rhenium Complexes Form Metal Carbenes from Cycloalkenes and Metal Carbynes from Alkanes. *J. Am. Chem. Soc.* **2007**, *129*, 6003−6016.
(96) Characteristic NMR shifts from in situ generation of **2-H$_3$** (245 K, 1,2-$F_2C_6H_4$): δ_H −10.84, −12.05 and −20.48; δ_P 49.0.
(97) Polymer below M_n = 5000 g/mol is at the limit of what can be accurately measured by GPC analysis under our conditions.
(98) Pattison, T. G.; Wang, S.; Miller, R. D.; Liu, G.; Qiao, G. G. 3D Nanoprinting via Spatially Controlled Assembly and Polymerization. *Nat. Commun.* **2022**, *13*, 1941.

https://doi.org/10.1021/acscatal.2c03778
ACS Catal. 2022, 12, 13050−13064